Photocatalysis
Research and Potential

SCIEPublish

Review

Review of Research on the Activation and Degradation of Antibiotics in Water by Photocatalysis Coupled with Persulfate

Wen Dong [1,†], Hongqing Song [1,†], Xuhui Wu [1], Ziqian Gao [1] and Qizhao Wang [1,2,*]

[1] College of Chemistry and Chemical Engineering, Northwest Normal University, Lanzhou 730070, China; 2865051207@qq.com (W.D.); 1176807906@qq.com (H.S.); 3298303808@qq.com (X.W.); 903801095@qq.com (Z.G.)
[2] School of Water and Environment, Chang'an University, Xi'an 710064, China

* Corresponding author. E-mail: qzwang@chd.edu.cn (Q.W.)

† These authors contributed equally to this work.

Received: 15 September 2026; Revised: 8 October 2026; Accepted: 6 November 2026; Available online: 19 November 2026

ABSTRACT: The widespread detection of antibiotics in aquatic environments and their potential threats to ecosystems and human health represent a significant global environmental issue. Sulfate radical-based advanced oxidation technologies (SR-AOPs) have garnered considerable attention because the activation of persulfate (PMS) produces various highly reactive oxygen species. In recent years, photocatalyst-coupled PMS activation systems have exhibited unique potential in antibiotic degradation, owing to their synergistic advantages of efficient separation of photo-generated charge carriers and targeted PMS activation. This review is structured around a three-dimensional analytical framework that includes "catalytic mechanism type—photocatalytic material system—reactive oxygen species generation pathways". It systematically examines the mechanistic characteristics and performance limitations of classical peroxymonosulfate (PMS) activation pathways, including transition-metal catalysis, carbon-based material catalysis, physical energy field activation, and electrocatalysis. Furthermore, it provides a comprehensive discussion of the thermodynamic foundations, kinetic regulation, and mechanisms of radical and non-radical competition involved in the photocatalytic activation of PMS. Building on this foundation, the review categorizes and assesses the latest advancements in the coupled activation of PMSs, addressing Type-II, Z-scheme, and S-scheme heterojunctions, as well as single-atom and diatomic catalysis, metal-organic framework (MOF) and covalent organic framework (COF)-based systems, and metal-free photocatalytic systems. To evaluate the advantages and limitations of photocatalytic coupling systems, along with future development directions, this review considers three key aspects: quantification of synergistic effects, adaptability to real water bodies, and engineering bottlenecks. This assessment aims to provide a systematic reference for material design and process optimization within this field.

Keywords: Photocatalysis; Peroxymonosulfate activation; Antibiotic degradation; Heterojunction; Single-atom catalyst; Reactive oxygen species; Advanced oxidation processes

© 2026 The authors. This is an open access article under the Creative Commons Attribution 4.0 International License (https://creativecommons.org/licenses/by/4.0/).

1. Introduction

As one of the most widely used drugs in the medical, livestock, and aquaculture sectors [1], the production and use of antibiotics have increased significantly over the past few decades [2]. However, traditional wastewater treatment processes demonstrate limited efficiency in removing antibiotics [3,4], resulting in the continuous discharge of substantial quantities of antibiotics and their metabolites into surface water, groundwater, and soil at concentrations ranging from ng/L to μg/L [5]. Sulfonamides, tetracyclines, and fluoroquinolones are the most frequently detected classes of antibiotics in aquatic environments due to their widespread use and high environmental persistence [6,7]. Residual antibiotics threaten ecological safety by promoting the spread of resistance genes and may also pose long-term cumulative risks to human health through exposure via drinking water and the food chain [8]. Therefore, developing efficient, cost-effective, and environmentally friendly technologies for treating antibiotic-contaminated wastewater holds significant practical importance.

Sulfate radical-based advanced oxidation technologies (SR-AOPs) have emerged as a promising alternative to the traditional Fenton reaction in recent years [9,10]. This shift is attributed to the advantages of the sulfate radical ($SO_4^{\bullet-}$), which include a high oxidation potential (E^0 = 2.5–3.1 V *vs*. NHE), a wide operational pH range (pH = 2–9), and a long half-life (30–40 μs) [11]. Persulfate (PMS, HSO_5^-), the primary oxidizing agent in SR-AOPs, possesses an asymmetric molecular structure that facilitates the activation of its O–O bond (with a bond energy of approximately 140–213 kJ/mol) more readily than that of persulfite (PDS, approximately 140–292 kJ/mol) and hydrogen peroxide (H_2O_2, approximately 213 kJ/mol) [12]. Furthermore, the activation pathways of PMS can be flexibly controlled through various activation methods [13,14].

Photocatalytic technology employs the generation of electron-hole pairs in semiconductors under light irradiation to activate peroxymonosulfate (PMS) [15,16]. This activation occurs either through the direct reduction of PMS by photo-generated electrons or through the indirect involvement of photo-generated holes in PMS transformation [2,17]. Compared to conventional PMS activation pathways, photocatalytic coupling systems present three significant advantages: (1) They utilize renewable light energy, eliminating the need for additional chemical reagents or high-energy inputs; (2) the efficient separation of photo-generated charge carriers facilitates simultaneous PMS activation and pollutant degradation; (3) the generation pathways of reactive oxygen species (ROS) can be adaptively modified through band structure engineering and interface regulation.

Several reviews have already surveyed parts of this field, and their scope defines the position of the present work. Ghanbari and Moradi [18] and Wang and Wang [19] summarized thermal, alkaline, radiation, transition-metal, and carbonaceous activation together with the associated mechanisms; Kohantorabi et al. [20] extended the coverage to supported metals, layered double hydroxides, MOFs, zeolites, and perovskites and compared radical with non-radical pathways; Zheng et al. [21] focused on heterogeneous activation by metal-based catalysts. Within individual material classes, biochar activation of PMS has been reviewed three times, covering active sites and activation mechanisms [22], influencing factors and catalyst reuse [23], and technical feasibility and life-cycle considerations for antibiotic removal [24]. For reactive species, the generation pathways and characterization methods of $^1O_2$ have been reviewed in detail [25], and ultrasound activation has been summarized in terms of synergy mechanisms and sonoreactor design [26,27], including a bibliometric analysis of the topic and a critical re-assessment arguing that the reported synergy is often overestimated [28,29]. These works address activation methods, material classes, or individual reactive species. A framework that compares the activation technologies on a single scale and places degradation performance alongside engineering scalability is still missing, and the present review is organized to fill that gap.

In this context, this review presents a three-dimensional analytical framework focused on “catalytic mechanism type—photocatalytic material system—reactive oxygen species generation pathway” to

systematically assess research advancements in the degradation of antibiotics in water through photocatalytic-coupled PMS activation. The text begins by utilizing established PMS activation pathways—namely, transition-metal catalysis, carbon-based material catalysis, physical energy field activation, and electrocatalysis—as benchmarks for comparing performance and mechanisms. It then delves into the electron transfer principles underlying photocatalytic PMS activation and clarifies the functional boundary of typical reactive oxygen species in the coupled system: $O_2^{\bullet-}$ may contribute to pollutant degradation, either directly for certain substrates or indirectly via conversion to other ROS, but its direct role should not be generalised. Subsequently, the review categorizes advancements in the coupled applications of heterojunction photocatalytic systems, single-atom and diatomic photocatalytic systems, and MOF/COF-based and metal-free photocatalytic systems. Finally, a comprehensive evaluation is performed across three dimensions: quantification of synergistic effects, identification of bottleneck challenges, and exploration of future directions.

2. The Basis of PMS Activation and Classic Activation Pathways

PMS (HSO_5^-), the active oxidizing component of potassium monopersulfate ($H_2O_2SO_3$), features an asymmetric O–O bond in its molecular structure. One end of this bond is connected to an SO_3 group, while the other end is linked to a hydrogen atom [30–32]. This asymmetry results in the bond energy of PMS's O–O bond, which ranges from approximately 140 to 213 kJ/mol, falling between that of H_2O_2 (approximately 213 kJ/mol) and that of PDS's O–O bond. However, thermodynamically, PMS is more readily reduced through single-electron transfer (Figure 1a). The activation of PMS requires the input of energy or electrons through various pathways, facilitating the cleavage of the O–O bond and leading to the generation of radical species centered on $SO_4^{\bullet-}$ or, via non-radical pathways, the production of $^1O_2$ and high-valent metal oxygen species [33,34]. Based on distinct activation mechanisms, classical PMS activation pathways are categorized into four major types: transition metal and spinel catalysis, carbon-based material catalysis, activation by physical energy fields, and electrocatalytic activation.

2.1. Molecular Characteristics and Activation Chemical Basis of PMS

Although PMS, PDS, and H_2O_2 are all members of the peroxide family, their molecular structural differences dictate their activation characteristics [35,36]. The asymmetric structure of PMS (HO-O-SO_3^-) renders it more polar than the symmetric PDS (-O_3S-O-O-SO_3^-), leading to increased electrophilic reactivity under identical conditions [37]. From a thermodynamic standpoint, the reduction potential of PMS, E^0 ($HSO_5^-/SO_4^{\bullet-}$) = +1.82 V *vs*. NHE, is lower than that of PDS (E^0 ($S_2O_8^{2-}/SO_4^{\bullet-}$) = +2.01 V) but higher than that of H_2O_2 (E^0 (H_2O_2/OH) = +1.78 V *vs*. NHE) [13,38]. The fundamental chemical principle underlying PMS activation is the cleavage mechanism of the O–O bond: Homolytic cleavage, in which both electrons are assigned to a single oxygen atom, primarily produces $SO_4^{\bullet-}$ and •OH radicals. In contrast, heterolytic cleavage, where one electron is assigned to a single oxygen atom, tends to generate high-valent metal-oxygen species (such as Fe(IV)=O and Co(IV)=O) or produce H_2O_2 through electron transfer [39]. His selectivity between homolytic and heterolytic cleavage establishes a theoretical foundation for the precise regulation of ROS generation pathways [40].

2.2. Catalytic Activation by Transition Metals and Spinel

The activation of peroxymonosulfate (PMS) by transition metal ions via the $M^{n+}/M^{(n+1)+}$ redox cycle represents one of the earliest identified classical activation pathways. Pioneering research conducted by Anipsitakis and Dionysiou [30,39] systematically examined the efficacy of transition metal ions, including Co^{2+}, Fe^{2+}, Cu^{2+}, Mn^{2+}, and Ni^{2+}, in activating PMS. Their findings revealed that Co^{2+} demonstrated the highest activation activity, with a reaction rate constant significantly surpassing that of the other metal ions. Nevertheless,

the homogeneous Co^{2+}/PMS system encounters challenges related to the recovery of metal ions and the potential for secondary pollution, which has led researchers to explore heterogeneous catalytic systems [41].

Spinel-type ferrites (MFe_2O_4, where M = Co, Cu, Mn, Zn, *etc*.) represent a significant class of materials for the catalytic activation of polyphase peroxymonosulfate (PMS) due to their exceptional magnetic separation properties and stable crystal structure [42]. $CoFe_2O_4$ efficiently activates PMS to generate sulfate ions (SO_4^{2-}) through the cycling of surface Co^{2+}/Co^{3+}, while the presence of Fe^{3+} in the spinel lattice effectively mitigates Co leaching (Figure 1b) [43–45]. $MnFe_2O_4$ further enhances electron transfer capacity through the synergistic interaction of Mn^{2+}/Mn^{3+} and Fe^{2+}/Fe^{3+} bimetallic species (Figure 1c) [46–48]. Additionally, Co–Mn bimetallic spinel ($CoMn_2O_4$) facilitates the regeneration of Co active sites via Mn species [49], resulting in more sustainable catalytic activity compared to single-metal oxides (Figure 1d) [50,51]. Recent research has also focused on modulating spinel catalytic activity through structural factors, including surface oxygen vacancies, lattice strain, and exposed crystal faces [52–54].

2.3. Catalytic Activation of Carbon-Based Materials

The activation of peroxymonosulfate (PMS) by carbon-based materials primarily occurs through non-radical pathways, thus addressing the challenge of metal leaching associated with transition metal catalysis [55,56]. Carbon materials with sp^2 hybridization, including carbon nanotubes (CNTs), graphene, mesoporous carbon, and biochar, facilitate electron transfer to PMS via electron-rich carbon networks (Figure 1f) [57]. The resulting reactive oxygen species (ROS) predominantly consist of singlet oxygen ($^1O_2$) or arise from direct electron transfer, rather than sulfate radicals (SO_4^{2-}) and hydroxyl radicals (OH) [58–60]. Research indicates that topological defects and edge carbon sites in CNTs serve as the primary active sites for PMS adsorption and activation (Figure 1e). Heteroatom doping significantly modulates the electronic properties of carbon materials. Specifically, graphitic nitrogen introduced through nitrogen doping enhances electron transfer efficiency by increasing the electron-donating capacity of the carbon framework [61]. In contrast, sulfur doping primarily promotes the generation of singlet oxygen ($^1O_2$) by regulating the concentration of defect sites [62]. Biochar has garnered considerable attention because of its diverse feedstock sources and low production costs; however, its catalytic activity depends on the interplay among pyrolysis temperature, oxygen-containing functional groups, defect concentration, and specific surface area [63,64]. Non-radical activation pathways in carbon-based materials demonstrate excellent resistance to anion interference in aqueous systems, yet they exhibit limited mineralization efficiency for high-concentration organic pollutants and typically necessitate combination with other activation pathways.

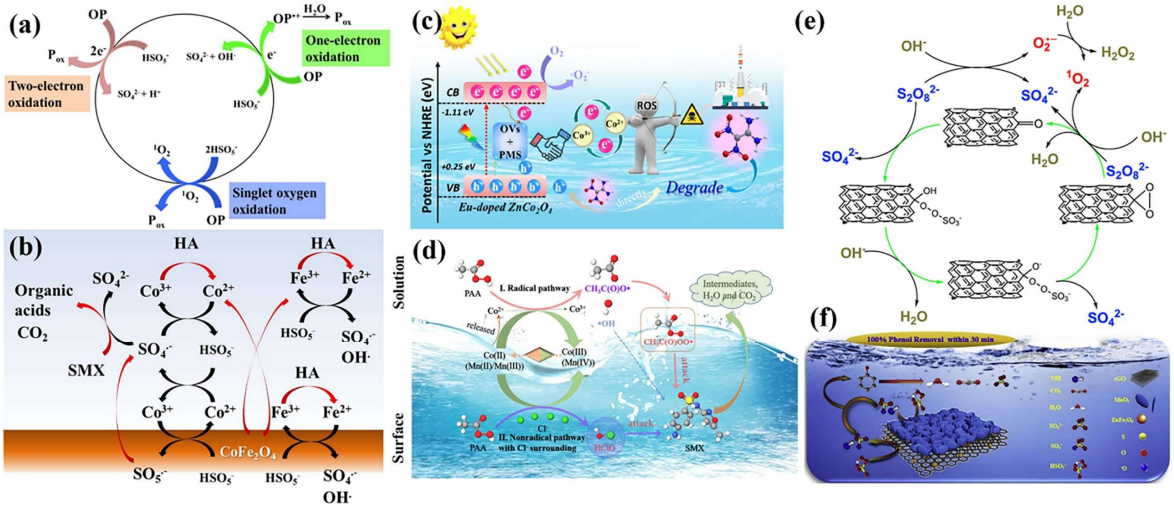

Figure 1. (**a**) The routes of PMS−induced direct oxidation of organic pollutants. OP and P_{ox} represent organic pollutants and oxidation products, respectively. (**b**) Proposed reaction mechanism for the SMX degradation by a $CoFe_2O_4$/PMS/HA system. (**c**)

The proposed photocatalytic mechanism for the Eu−doped $ZnCo_2O_4$. (**d**) The proposed photocatalytic mechanism for the $Co_{3-x}Mn_xO_4$. (**e**) The proposed photocatalytic mechanism for the Carbon Nanotube. (**f**) The proposed mechanism of phenol degradation in the γ−MnO_2 @$ZnFe_2O_4$/rGO nanohybrid/PMS system. Reprinted from ref. [13]. Reprinted from ref. [43]. Reprinted from ref. [48]. Reprinted from ref. [50]. Reprinted from ref. [55]. Reprinted from ref. [57].

2.4. Physical Energy Field and Electrocatalytic Activation

The physical energy field breaks the O–O bond by directly supplying energy to the PMS molecule, eliminating the need for a catalyst. Thermal activation adheres to the Arrhenius equation, with an activation energy of approximately 100–200 kJ/mol. The reaction temperature generally must exceed 60 °C to attain a significant PMS conversion efficiency [65]. Photolysis at 254 nm generates $SO_4^{\bullet-}$ and OH by directly exciting the O–O bond in PMS, with a quantum yield of approximately 0.5–1.0. However, the penetration depth of UV light is limited, and energy consumption remains high. Ultrasonic activation uses the localized high temperatures (approximately 5000 K) and high pressures (approximately 1000 atm) produced by cavitation to facilitate rapid PMS decomposition. The collapse of cavitation bubbles releases a substantial amount of energy within microseconds [26]. Microwave-assisted activation integrates both thermal and non-thermal effects, significantly enhancing the efficiency of PMS activation and reducing reaction time [66].

Electrocatalytic activation of Persulfate (PMS) occurs through electrode reactions. At the anode, sulfate ions (SO_4^{2-}) undergo direct oxidation to generate sulfate radicals ($SO_4^{\bullet-}$). Concurrently, at the cathode, oxygen (O_2) is reduced *in situ* to produce hydrogen peroxide (H_2O_2), which further activates PMS, establishing a synergistic pathway of "anodic oxidation + cathodic activation" [67,68]. This method provides advantages such as enhanced reaction controllability and the feasibility of continuous processing. However, the primary limitations currently lie in the costs associated with electrodes and energy consumption.

3. Electron Transfer Mechanism of Photocatalytically Activated PMS

The primary characteristic that differentiates the photocatalytic activation of PMS from traditional dark activation is the involvement of both photo-generated electrons and holes in the PMS activation process (Figure 2a,b) [69]. When a semiconductor is excited by photons with energy exceeding its bandgap width, electrons in the valence band transition to the conduction band, resulting in the formation of holes in the valence band. Electrons (e^-) in the conduction band exhibit significant reducing power and can directly reduce PMS to $SO_4^{\bullet-}$ ($HSO_5^- + e^- \rightarrow SO_4^{\bullet-} + OH^-$) (Figure 2c) [70]. The hole (h^+) in the valence band exhibits strong oxidative properties, enabling it to oxidize PMS to produce $SO_5^{\bullet-}$ ($HSO_5^- + h^+ \rightarrow SO_5^{\bullet-} + H^+$), which can subsequently be converted to O_2 (Figure 2d) [71]. Consequently, the efficiency of photo-generated carrier separation in the photocatalytic system directly influences the activation performance of PMS.

Dissolved oxygen (O_2) can be reduced to the superoxide OH (O_2^-) through the action of conduction band electrons. The superoxide anion can either directly degrade pollutants or be converted to hydrogen peroxide (H_2O_2) via dismutation or hole oxidation (Figure 2e–g) [72]. The relationships among the formation and transformation of these reactive oxygen species (ROS) create a complex reaction network within the photocatalytically activated persulfate (PMS) system. Regulating this network necessitates multidimensional approaches, including band engineering, surface modification, and optimization of operating parameters [73].

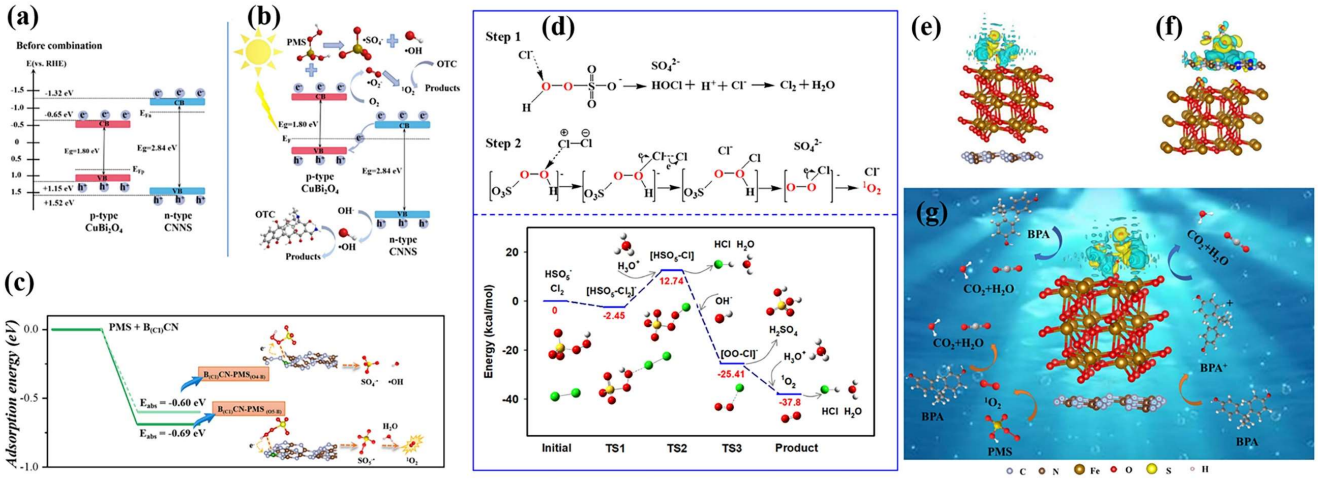

Figure 2. (**a**) The band structure diagrams of $CuBi_2O_4$ and CNNS; (**b**) The possible degradation mechanism in the 10% CNNS/$CuBi_2O_4$ + PMS + Vis system. 25 unique mechanisms of reactive species production from PMS activation by the free-metal BCN could be proposed in (**c**), (**d**) Proposed mechanisms of $^1O_2$ formation from the interaction of PMS and Cl^- in aqueous solution. (**e**,**f**) charge density difference in Fe_2O_3/g −C_3N_4−2; (**g**) possible mechanism of contaminant degradation in the PMS/Fe_2O_3/g−C_3N_4−2 system. Reprinted from ref. [69]. Reprinted from ref. [70]. Reprinted from ref. [71]. Reprinted from ref. [72].

3.1. Band Matching and PMS Activation Thrmodynamics

The thermodynamic feasibility of photocatalytic activation of peroxymonosulfate (PMS) relies on the relationship between the band positions of the semiconductor and the redox potential of PMS. For the transfer of electrons from the conduction band to PMS to be thermodynamically favorable, the conduction band minimum (CBM) must be more negative than the reduction potential of PMS (E^0 ($HSO_5^-/SO_4^{\bullet-}$) = +1.82 V *vs*. NHE) [69]. Both TiO_2 (CBM ≈ −0.3 V *vs*. NHE) and g-C_3N_4 (CBM ≈ −1.2 V *vs*. NHE) meet this criterion; however, g-C_3N_4 provides a stronger driving force for electron reduction due to its more negative conduction band position. Wide-bandgap semiconductors, such as TiO_2 (Eg ≈ 3.2 eV), are thermodynamically feasible but can only be excited by ultraviolet light, which restricts the utilization of visible light. The valence band maximum (VBM) plays a critical role in the oxidative activation of peroxymonosulfate (PMS). If the VBM exceeds the oxidation potential of PMS, holes can directly oxidize PMS to generate $SO_5^{\bullet-}$. Bi-based oxides, such as Bi_2WO_6, which has a VBM of approximately +3.0 V *vs*. NHE, demonstrate a strong capacity to oxidize PMS through hole-mediated processes due to their highly positive VBM. Consequently, the ideal objective in photocatalyst design is to create a material whose band positions fulfill the dual requirements of reducing PMS via the conduction band and oxidizing PMS via the valence band.

3.2. Carrier Separation and PMS Activation Kinetics

Thermodynamic feasibility serves as a prerequisite; however, the migration rate of photo-generated charge carriers to the PMS molecules at the interface constitutes the kinetic bottleneck that dictates PMS activation efficiency. The rapid recombination of photo-generated electrons and holes, both in the bulk and at the surface, primarily limits the efficiency of photocatalytic PMS activation [73]. Previous studies demonstrate that surface modification strategies, including co-catalyst loading and oxygen/nitrogen vacancy defect engineering, effectively promote carrier separation and accelerate electron transfer to the PMS [70]. Introducing nitrogen vacancies into g-C_3N_4 nanosheets creates intermediate energy levels within the bandgap, which significantly enhances carrier separation efficiency and reduces interfacial charge transfer resistance [72].

The construction of heterostructures represents a crucial strategy for effectively coupling carrier separation with PMS activation. A heterojunction formed between two semiconductors with compatible bandgap widths and band positions generates an intrinsic electric field that drives photo-generated electrons and holes to migrate in opposite directions, thereby effectively suppressing carrier recombination [73]. Transient photocurrent response measurements and electrochemical impedance spectroscopy (EIS) serve as the most direct electrochemical methods for evaluating carrier separation efficiency and interfacial charge transfer performance. Additionally, time-resolved fluorescence spectroscopy and surface photovoltage spectroscopy provide insights into carrier transport kinetics across various time scales.

3.3. Competition Mechanism Between Free Radical and Non-Radical Pathways

In a photocatalytically activated PMS system, the competition between radical pathways ($SO_4^{\bullet-}$, •OH, $O_2^{\bullet-}$) and non-radical pathways ($^1O_2$, high-valent metal oxygen species, direct electron transfer) determines the degradation mechanism and mineralization efficiency [71]. This competitive relationship is regulated by the surface properties of the catalyst and the reaction conditions. The electron density and types of defects at the active sites on the catalyst surface decisively influence the adsorption configuration of PMS. Metal-center sites with unsaturated coordination tend to adsorb PMS through terminal oxygen, which promotes the heterolytic cleavage of the O–O bond, resulting in the formation of high-valent metal-oxygen species. In contrast, defect sites with lower electron density typically adsorb PMS via side oxygen, leading to homolytic cleavage and the formation of $SO_4^{\bullet-}$ [72]. Among the operational parameters, pH and PMS concentration exert the most significant effects. Under weakly alkaline conditions (pH = 8), the decomposition rate of PMS decreases, leading to an increased contribution from non-radical pathways, such as $^1O_2$ and electron transfer. Dissolved oxygen concentration indirectly influences $^1O_2$ production by regulating the generation of O^{2-}. Precise control of the reaction pathways holds significant engineering importance for enhancing treatment efficiency and optimizing PMS utilization. While the radical pathway exhibits high reactivity, it is vulnerable to quenching by the aquatic matrix. In contrast, the non-radical pathway demonstrates considerable resistance to interference but has relatively low mineralization efficiency. The synergy between these two pathways is anticipated to yield optimal degradation outcomes.

4. Heterojunction Photocatalytic System Coupled with PMS Activation

Research on the photocatalytic activation of peroxymonosulfate (PMS) indicates that single-semiconductor photocatalysts typically encounter challenges, including high rates of photo-generated carrier recombination and limited PMS activation efficiency. Constructing heterostructures serves as a crucial strategy to overcome these limitations. Heterojunctions can be categorized into three primary types based on variations in band alignment and charge transfer pathways: Type-II, Z-scheme, and S-scheme [74,75]. Each configuration offers a unique basis for material design, facilitating PMS activation through distinct mechanisms of carrier separation.

4.1. Carrier Separation and PMS Activation of Type-II Heterojunction System

A Type-II heterojunction comprises two semiconductors with distinct bandgap widths and band positions. Upon photoexcitation, electrons in the conduction band migrate from semiconductor I, which possesses a more negative potential, to semiconductor II, characterized by a more positive potential. Concurrently, holes in the valence band move in the opposite direction toward semiconductor I, facilitating space charge separation. In this arrangement, electrons accumulate in semiconductor II, which exhibits a lower absolute value of the conduction band minimum (CBM), leading to a reduced reducing capacity; nonetheless, this capacity remains adequate to reduce PMS and generate $SO_4^{\bullet-}$. For instance, in the Bi_2WO_6/BiOCl heterojunction, the CBM of Bi_2WO_6 (approximately +0.46 V *vs*. NHE) is more positive than that of BiOCl

(approximately −1.0 V *vs*. NHE). Following the transfer of photo-generated electrons from BiOCl to the conduction band of Bi_2WO_6, these electrons effectively activate PMS, resulting in a degradation rate constant for tetracycline that is 4 times greater than that of pure Bi_2WO_6 (Figure 3a,b). The 2D/2D g-C_3N_4/BiOBr heterojunction significantly accelerates inter-interface carrier transport due to its large-area contact interface (Figure 3e). Similarly, the 2D/2D g-C_3N_4/BiOBr heterojunction significantly accelerates the cross-interface transfer of charge carriers through a large-area contact interface. The kinetic constant for PMS activation to degrade sulfamethoxazole under visible light is increased by several times compared with those of g-C_3N_4 and BiOBr monomers, respectively (Figure 3c,d). However, the inherent limitation of Type-II heterojunctions, dictated by their sacrificial redox potential, results in reactive oxygen species (ROS) that are predominantly $SO_4^{\bullet-}$ and OH^-, with relatively limited contributions from non-radical pathways. This limitation may constrain their effectiveness in water bodies characterized by high matrix interference.

4.2. Applicability Boundaries and Cross-Interference of Reactive-Species Identification Methods

The assignment of radical versus non-radical contributions in photocatalysis-coupled PMS systems relies mainly on three families of methods: quenching (scavenging) experiments, EPR spin trapping, and probe-compound assays. Each method has applicability boundaries, and evidence from a single method is prone to cross-interference [76]. Quenching experiments infer the contribution of a species from the suppression of degradation after a selective scavenger is added; their reliability depends on the ratio of the scavenger rate constants toward the target and the interfering species. Methanol is often used to scavenge both $SO_4^{\bullet-}$ and •OH, but its ability to distinguish them is limited: its rate constant with •OH (about 10^9 $M^{-1}s^{-1}$) exceeds that with $SO_4^{\bullet-}$ (about 10^7 $M^{-1}s^{-1}$) by only about two orders of magnitude, so methanol suppression can serve only as qualitative evidence for a radical pathway and cannot apportion the two radicals [77]. tert-Butanol is more selective for •OH and is often combined with methanol to distinguish •OH from $SO_4^{\bullet-}$, yet its own competing reaction with the target still requires control experiments.

The identification of $^1O_2$ suffers similar interference. Common $^1O_2$ quenchers such as furfuryl alcohol, sodium azide and histidine react directly with PMS and are consumed, so suppressed degradation can reflect depletion of the oxidant rather than $^1O_2$ quenching [78]. In carbon-based/PMS systems, furfuryl alcohol inhibition is more closely related to its competing reaction with $SO_4^{\bullet-}$, which tends to overestimate the $^1O_2$ contribution; conclusions that distinguish $^1O_2$ from mediated electron transfer on the basis of scavenger experiments therefore need reassessment [79,80]. EPR spin trapping identifies radicals from the hyperfine splitting of the adducts formed with spin traps such as DMPO, but the DMPO-OH signal can also arise from direct oxidation or nucleophilic addition of DMPO, and a weak or absent signal cannot exclude the presence of radicals, so the assignment of $SO_4^{\bullet-}$ versus •OH remains uncertain [76,81].

In view of these limitations, a multi-technique evidentiary standard is recommended for reactive-species assignment: the conclusion that a species dominates should be supported by at least two mutually independent techniques (for example, quenching combined with EPR, or probe-compound kinetics combined with *in situ* spectroscopy), reported under identical reaction conditions with the scavenger concentration, dosing order and control experiments stated. For high-valent metal-oxo species and electron-transfer pathways, conventional quenching experiments provide little reliable evidence, and *in situ* Raman spectroscopy, isotope labeling, electrochemical impedance, and competition kinetics are needed to constrain them. Where direct evidence is lacking, the relevant species are better described as possible or minor, rather than assigning precise contributions that cannot be verified [76,77].

4.3. Z-Scheme Heterojunction Coupled PMS Activation

In a Z-scheme heterojunction, photo-generated electrons from Semiconductor I recombine with photo-generated holes from Semiconductor II through a conductive medium, such as Au, Ag, conductive carbon

materials, or direct contact at the solid-state interface. This process retains the strongly reducing electrons from Semiconductor II and the strongly oxidizing holes from Semiconductor I, thereby achieving both high reducing and high oxidizing capabilities simultaneously [17]. This configuration offers a broader potential window for multi-path activation of PMS. The strong reducing electrons on the Semiconductor II side can efficiently reduce PMS to produce $SO_4^{-}\cdot$, while the strong oxidizing holes on the Semiconductor I side can directly oxidize PMS to generate $SO_5^{\bullet-}$, which is subsequently converted to H_2O_2.

The C-$LaFeO_3$/Co-doped g-C_3N_4 direct Z-scheme heterojunction facilitates Z-type carrier migration via direct solid-state interface contact. Under visible light, the reaction rate constant for PMS-catalyzed tetracycline degradation is 7 times greater than that of the dark-state PMS system, with •OH and $SO_4^{\bullet-}$ acting as the primary active species (Figure 3f,g). The primary challenges in Z-scheme configurations involve the encapsulation strategy for the conductive medium and the optimization of ohmic contacts at the interface. Inadequate interface engineering can lead to carrier recombination within the conductive medium instead of facilitating conduction across the interface, ultimately diminishing photocatalytic efficiency.

4.4. Interface Electronic Control and PMS Activation of S-Scheme Heterojunction

The S-scheme heterojunction (Step-scheme) represents a novel type of heterostructure that has gained attention in recent years. Its defining characteristic is the intrinsic electric field generated at the interface between two n-type semiconductors, which results from the disparity in their Fermi levels. Before contact, the oxidized photocatalyst (OP) possesses a positive band gap and a lower Fermi level, whereas the reduced photocatalyst (RP) exhibits a negative band gap and a higher Fermi level. Following contact, electrons flow spontaneously from the RP to the OP until the Fermi levels reach equilibrium, thereby establishing an intrinsic electric field at the interface that directs from the RP to the OP [82]. The built-in electric field drives the recombination of excess electrons in the OP conduction band with excess holes in the RP valence band, while retaining the most reducing electrons in the RP conduction band and the most oxidizing holes in the OP valence band. This process achieves optimal kinetic and thermodynamic conditions for PMS activation.

The $MnFe_2O_4$/MoS_2 S-scheme heterojunction achieves 89.57% efficiency in degrading ofloxacin through PMS activation under visible light (Figure 3h–j). DFT calculations indicate that Fe–S bonds at the interface reduce the carrier migration barrier, thereby accelerating electron transfer from the MoS_2 conduction band to $MnFe_2O_4$. Reports of comparable systems are accumulating: a 1D/2D CoNi-LDH/$ZnIn_2S_4$ S-scheme heterojunction degrades tetracycline more efficiently than its single components under photocatalytic-PMS activation [33]; $BiVO_4$/Cu-TCPP accelerates carrier transport through an interfacial built-in field for ultrafast ciprofloxacin degradation [83]; and MoO_{3-x}@MoS_2 strengthens PMS activation through oxygen vacancies and Mo^{4+}/Mo^{5+}/Mo^{6+} redox cycling [84]. The common feature of these systems is that the interfacial built-in field retains the most reducing conduction-band electrons and the most oxidizing valence-band holes, making both the reductive generation of $SO_4^{\bullet-}$ and the oxidative generation of $SO_5^{\bullet-}$ accessible [85].

The three heterojunction configurations differ systematically in PMS activation pathway selectivity [86]. Type-II heterojunctions rely on spatial charge separation, with electrons and holes migrating to band positions of reduced reducing and oxidizing power, so the reactive oxygen species are dominated by radicals such as $SO_4^{\bullet-}$ and •OH, with limited driving force for non-radical pathways such as high-valent metal-oxo species and $^1O_2$. Z-scheme heterojunctions broaden the ROS spectrum by retaining strongly reducing electrons and strongly oxidizing holes, and radical and non-radical pathways often coexist; metal-based Z-scheme systems frequently show higher $SO_4^{\bullet-}$ and $^1O_2$ contributions [17], whereas metal-free Z-scheme systems (such as PPy/MCN) maintain the synergy of photocatalysis and PMS activation while avoiding metal leaching [87]. S-scheme heterojunctions further exploit a Fermi-level-driven interfacial built-in field to retain strong redox capability and improve carrier utilization, often giving higher $SO_4^{\bullet-}$ yields and a more pronounced direct hole-oxidation contribution. The differences can be summarized as

follows: Type-II excels at separation efficiency at the cost of redox potential; Z-scheme excels at potential retention but depends on interface contact quality; S-scheme attempts a balance, and whether its gain materializes depends on the strength and stability of the interfacial built-in field.

Heterojunction photocatalytic systems coupled with PMS activation combine clear advantages with notable limitations. The advantage lies in band-aligned spatial charge separation, which raises PMS activation and photo-generated carrier utilization without increasing oxidant dosage and allows the ROS spectrum to be tuned by configuration choice. The limitations center on a strong dependence on interface quality: interface defects, lattice mismatch, and imperfect encapsulation of the conductive medium cause carriers to recombine at the interface rather than migrate directionally; the potential sacrifice of Type-II, the interface-engineering complexity of Z-scheme and the requirement for built-in-field stability in S-scheme jointly limit reliability in long-term operation. Open questions include how to confirm the actual charge-transfer pathway of the Z-scheme and S-scheme at the atomic scale rather than inferring it from band positions, how to keep the interface stable in real water, and how to establish a quantitative correspondence between configuration and PMS activation pathway selectivity [85,86].

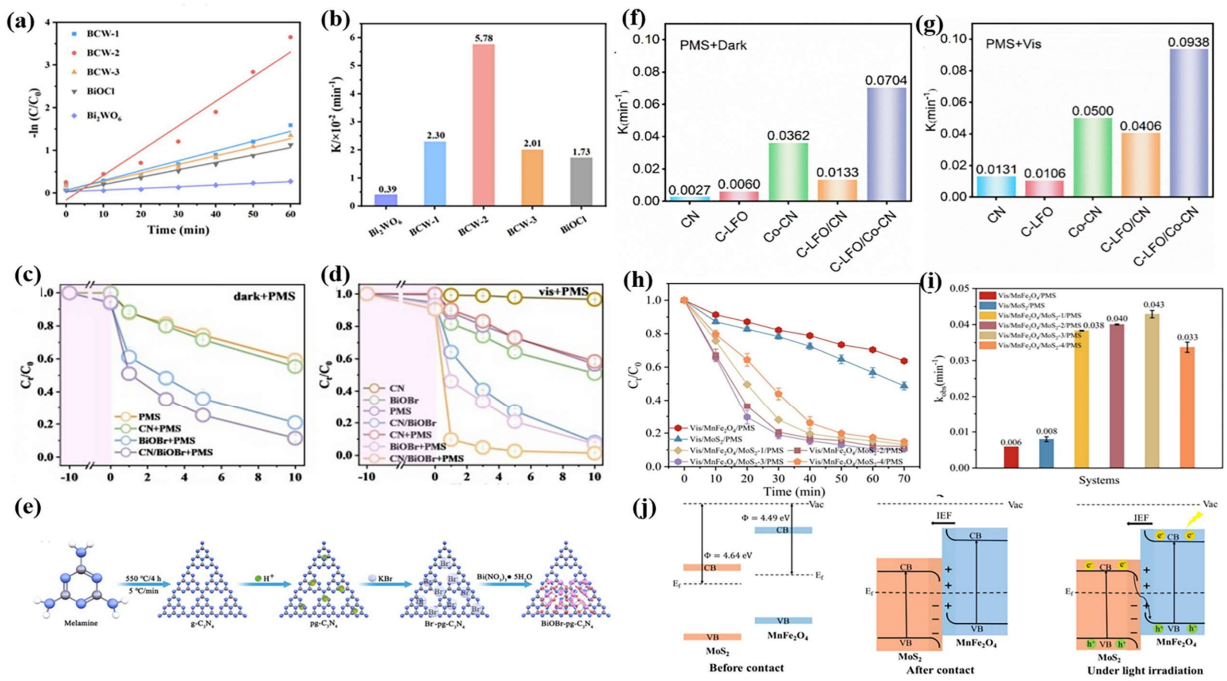

Figure 3. (**a**) Pseudo−first−order kinetic fitting curves for different samples; (**b**) Apparent rate constants for all samples; Degradation effects of different catalytic systems (**c**) in dark conditions and (**d**) under visible light irradiation. (**e**) Schematic diagram illustrating the synthesis of CN/BiOBr heterojunction. Apparent degradation rate constants of NOR within the initial 30 min over different catalysts under various activation conditions: (**f**) PMS activation, and (**g**) combined PMS-Vis activation. Ofloxacin degradation efficiencies (**h**) and k_{obs} values (**i**); schematic diagram of the band configuration before contact, after contact in the dark, and photo-generated charge carrier transfer process (**j**). Reprinted from ref. [74]. Reprinted from ref. [75]. Reprinted from ref. [17]. Reprinted from ref. [82].

5. Single-Atom and Di-Atom Catalytic Photosystems

Single-atom catalysts (SACs) exhibit 100% atomic utilization efficiency of metal atoms and allow for precisely controllable coordination environments, positioning them at the forefront of atomic-level catalyst design [88]. In the field of photocatalytic coupling for PMS activation, single-atom catalysts (SACs) achieve selective control over activation pathways by transitioning from radical-mediated to non-radical-mediated mechanisms, which include high-valent metal-oxygen species, singlet oxygen ($^1O_2$), and electron

transfer. This unique electronic structure has facilitated significant advancements in recent years [89,90]. This section addresses three key aspects: the regulation of activation pathways by the coordination environment, the relationship between the type of metal center and activation selectivity, and the phenomenon of diatomic synergy.

5.1. Regulation of PMS Activation Pathways by Coordination Environment

The coordination environment at a single-atom site directly influences the adsorption configuration of PMS and the O–O bond cleavage pathway by modulating the electron density and the position of the d-band center of the metal center [91,92]. Using a single Co atom as an example, the Co–N_4 coordination configuration exhibits a moderate d-band center for Co. In this arrangement, PMS tends to adsorb at the Co site through terminal oxygen, which facilitates the heterolytic cleavage of the O–O bond and results in the formation of the higher-valent Co(IV)=O species instead of the $SO_4^{\bullet-}$ radical. When the coordination environment shifts to Co–N_3, the increased coordination unsaturation diminishes the electron density of Co, prompting the PMS adsorption configuration to transition toward a side-oxygen mode. This change enhances homolytic O–O bond cleavage and fosters the formation of radical pathways. Coordination engineering of Fe single atoms demonstrates similar regulatory patterns: Fe–N_4 sites typically yield the higher-valent Fe(IV)=O species, while Fe–N_2O_2 or Fe–N_3 sites are more inclined toward radical pathways [93]. Consequently, designing the coordination environment emerges as a crucial strategy for precisely regulating PMS activation pathways.

5.2. Metal Center Types and Activation Selectivity

Different transition metal single-atom sites demonstrate distinct selectivity for the activation of peroxymonosulfate (PMS). Experimental results and density functional theory (DFT) calculations indicate that cobalt (Co) single-atom sites predominantly facilitate non-radical pathways through the mediation of high-valent Co(IV)=O species [94]. In contrast, iron (Fe) single-atom sites exhibit the ability to switch flexibly between radical and non-radical pathways, influenced by the coordination environment and pH conditions. Under acidic conditions, high-valent Fe(IV)=O species are predominant, while under basic conditions, the contribution of singlet oxygen ($^1O_2$) increases [93]. The high redox cycling activity of Cu(I)/Cu(II) allows Cu single-atom sites to primarily activate peroxymonosulfate (PMS) through a radical pathway. In contrast, Ni–N_4 single-atom sites activate PMS via a dual, non-radical synergistic pathway involving direct electron transfer and high-valent Ni(IV)=O species. This mechanism demonstrates exceptionally high atomic efficiency and PMS utilization in the degradation of sulfamethoxazole [95]. Conversely, Mn single-atom sites show relatively low activation activity due to the instability of the Mn(III)/Mn(IV) cycle [96,97].

These conclusions on metal-center selectivity come from two distinct evidence sources, and distinguishing them helps to judge the reliability of the conclusions. Some rest primarily on density functional theory (DFT) calculations, which predict pathway selectivity by comparing the PMS adsorption energy, d-band center, and O–O bond activation barrier across metal sites [98]. Others are supported by experiment, including X-ray absorption spectroscopy (XANES/EXAFS) and aberration-corrected electron microscopy to confirm single-atom site structure, *in situ* spectroscopy to trap high-valent metal-oxo species, and isotope labeling to trace oxygen-transfer pathways. For Co–N_4 sites, the mechanism of selective oxidation via radical and non-radical pathways was established by experiment and theory together [99]; whereas the study of Cu single atoms activating PMS for oxytetracycline degradation relied mainly on structural characterization by XANES/EXAFS [100]. Because both purely theoretical and experimentally validated systems coexist in the literature, the evidence type should be noted when citing pathway-selectivity conclusions.

5.3. Diatomic Synergistic Effect and Ultra-Efficient PMS Activation

Dual-atom catalysts (DACs) overcome the linear proportionality constraints associated with single-atom sites by leveraging electronic synergy between neighboring metal centers. This synergy enhances the overall processes of PMS adsorption, activation, and electron transfer. The strong electronic coupling between Fe and Co in the Fe–Co bimetallic catalyst ($FeCoN_6$) produces a synergistic effect akin to that observed in natural enzyme catalysis. In this system, Co sites preferentially adsorb peroxymonosulfate (PMS) and facilitate its activation, while Fe sites sustain the high-activity state of the Co sites through electronic regulation. This synergistic mechanism induces a novel surface collision oxidation pathway, leading to an electron transfer efficiency of nearly 100% for PMS [101]. An MXene-based Fe–Co metal pair array facilitates the directed cleavage of O–O bonds in PMS through asymmetric coordination, thereby enabling selective control over the formation pathways of high-valent metal-oxygen species [102]. A synergistic system comprising Co single atoms and clusters modulates the electronic structure of the single-atom Co sites through the clusters, resulting in ultra-high PMS utilization and enhanced antibiotic degradation rate constants [103].

6. MOF/COF-Based and Metal-Free Photocatalytic Systems

Metal-organic frameworks (MOFs) and covalent organic frameworks (COFs) serve as unique photocatalytic platforms for activating peroxymonosulfate (PMS) because of their tunable pore structures, high specific surface areas, and customizable metal/ligand compositions. In contrast, metal-free photocatalysts, such as g-C_3N_4 and its derivatives, do not contain metal components, which eliminates the problem of metal leaching. Recently, defect engineering and heteroatom doping have successfully broadened their response range to visible light [70,104].

6.1. MOF-Based Photocatalytic Activation of PMS

The primary advantage of metal-organic frameworks (MOFs) in the photocatalytic coupling of peroxymonosulfate (PMS) activation is that, upon illumination, ligand-to-metal charge transfer (LMCT) occurs at metal-oxygen cluster nodes. This process results in the *in situ* reduction of high-valent metal ions, such as Fe(III) to Fe(II) and Ti(IV) to Ti(III), thereby accelerating the metal redox cycle and enhancing PMS activation (Figure 4a–c) [105]. Bimetallic metal-organic frameworks (MOFs), such as CuCo-MOF, achieve enhanced activation of peroxymonosulfate (PMS) through the synergistic interaction of two metal sites (Figure 4d–f). The copper site functions as the primary photo-generated electron acceptor, whereas the cobalt site acts as the catalytic active center for PMS activation. This spatial synergy improves both electron transfer efficiency and the rate of PMS activation (Figure 4g,h) [106].

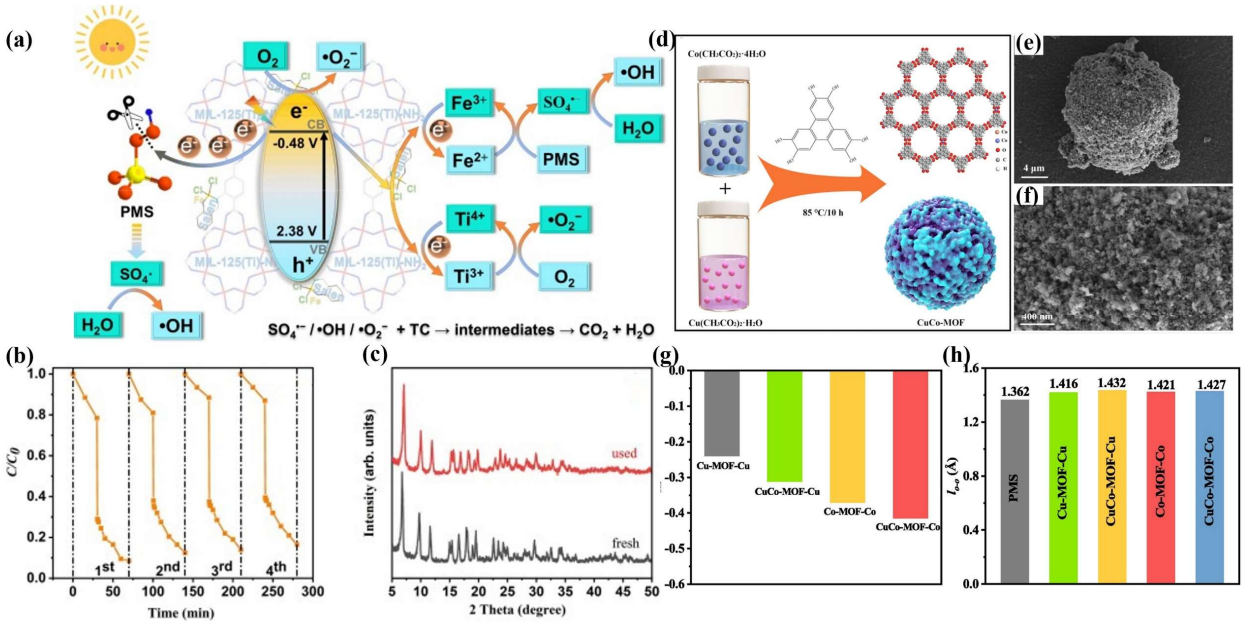

Figure 4. (**a**) Possible mechanism for TC degradation by MSF/PMS/Light system. (**b**) Reusability experiments over MIL−125(Ti)−NH_2–Sal−Fe for TC degradation. Condition: [photocatalyst] = 0.1 g/L, [PMS] = 0.7 mM, pH = 4.5 and [TC] = 0.02 g/L; (**c**) PXRD patterns; (**d**) Schematic illustration for the preparation of CuCo-MOF. (**e**,**f**) SEM images of CuCo-MOF at different magnifications; (**g**) Adsorption energy of PMS on metal sites of different structures; and (**h**) bond length of peroxy bonds (l_{O-O}) in the PMS. Reprinted from ref. [105]. Reprinted from ref. [106].

MOF-derived carbon materials retain the pore structure of MOFs through high-temperature carbonization and incorporate nitrogen doping, resulting in excellent electron-transfer performance during PMS activation [107]. However, Single-atom and diatomic catalytic photosystems offer advantages and limitations. The advantages are near-100% atomic utilization, a well-defined active-site structure that supports atomic-level structure-activity relationships and selective control from radical toward non-radical pathways, and diatomic synergy that overcomes the proportional-relationship constraint of a single metal site. The limitations are that single-atom sites are prone to aggregation and loss in long-term oxidizing environments, with stability highly sensitive to the support and coordination environment; that the high-selectivity conclusions often depend on a combination of DFT predictions and *in situ* characterization, and differences in computational models and experimental conditions hamper cross-study comparison; and that synthesis cost and scale-up remain practical obstacles. Open questions include the long-term stability mechanism of single-atom sites in real water, direct experimental evidence for the diatomic synergistic electron-transfer pathway, and translating high-selectivity mechanisms into scalable synthesis processes.

6.2. Metal-Free Photocatalyst Defects and Doping Engineering

As a representative metal-free visible-light catalyst, g-C_3N_4 attracts significant attention in the field of photocatalysis-PMS coupling due to its tunable electronic structure and thermal and chemical stability. However, the photocatalytic activity of pristine g-C_3N_4 is constrained by a high rate of photo-generated carrier recombination and a narrow range of visible-light absorption. Defect engineering and heteroatom doping serve as effective strategies for enhancing the performance of g-C_3N_4 in activating peroxymonosulfate (PMS). Introducing nitrogen vacancies generates defect states within the g-C_3N_4 bandgap, enhancing the n→π* electronic transition and extending visible-light absorption beyond 600 nm. Concurrently, the adsorption energy of PMS at these defect sites decreases significantly, resulting in a notable improvement in PMS activation efficiency [70]. Boron doping shifts the conduction band position of g-C_3N_4 upward, which enhances the reducing ability of the conduction band electrons and increases the

thermodynamic driving force for the reduction of PMS to $SO_4^{\bullet-}$ as a result of PMS reduction. As a homologue of g-C_3N_4, g-C_3N_5 exhibits superior light absorption and PMS activation capabilities compared to g-C_3N_4 in visible-light-PMS coupling systems. This superiority arises from its narrower bandgap (approximately 1.9 eV) and more negative conduction band potential [108]. Furthermore, g-C_3N_4 modified with carbon quantum dots (CQDs) significantly enhances carrier separation via interfacial charge transfer. Nevertheless, the overall catalytic activity of the metal-free catalyst remains considerably lower than that of the metal-based catalyst, particularly evident in the differences in the PMS activation rate constant and the pollutant mineralization rate. The accurate identification of atomic-level active sites, along with the stability challenges associated with high vacancy concentrations, continues to pose significant bottlenecks.

MOF/COF-based and metal-free photocatalysts offer tunable pores, designable composition, and environmental friendliness, alongside clear limitations. The advantage is that MOFs allow molecular-level design of the light response and active sites through their metal nodes and linkers, while metal-free catalysts avoid metal leaching at the source; the limitations are that MOF hydrolytic stability and photocorrosion restrict long-term operation, and metal-free catalysts lag metal-based systems in catalytic activity, active-site density, and mineralization. Open questions include quantitative stability data for MOF/COF under PMS oxidation (rather than activity retention over only a few cycles), on-line monitoring methods for photocorrosion and metal leaching, and accurate identification of active sites in metal-free catalysts together with the stability trade-off posed by high vacancy concentrations.

7. Advantages, Boundaries and Challenges of Photocatalytic Coupling Systems

Building on the systematic review of classical activation pathways and diverse photocatalytic coupling systems, including heterojunctions, single-atom/dual-atom catalysis, MOF/COF-based systems, and metal-free systems, this section evaluates the optimal boundaries and applicable conditions for PMS activation through photocatalytic coupling. This evaluation is conducted from three perspectives: quantification of synergistic effects, analysis of key bottlenecks, and development of mitigation strategies.

7.1. Quantification of Synergy Effects and Applicable Conditions

The synergy factor ($SF = k_{photo+PMS}/(k_{photo} + k_{PMS})$) compares the apparent rate constant of the combined system with the sum of the rate constants of the two individual processes, to test whether coupling produces an additional gain; an SF greater than 1 indicates positive synergy [109]. The definition presumes that k_{photo}, k_{PMS} and $k_{photo+PMS}$ are measured under identical light, oxidant dose and water matrix, and that photocatalysis and PMS activation are independent and additive. When these premises fail, the physical meaning of SF becomes unclear: the denominator is the sum of two single-process rate constants, and although its dimension matches the numerator, the ratio deviates from the true degree of synergy when k_{photo} is measured in the dark or at a different light intensity. Moreover, SF is defined inconsistently across studies, some using the ratio of rate constants, some the ratio of removal efficiencies, and some a fold-increase relative to a single process, so cross-study comparison lacks a common basis [81]. SF is therefore best used as a relative index within a single study, not as an absolute criterion across systems or literature.

7.2. Supplementary Performance Indicators

Because of these limitations, SF alone is insufficient to judge the merit of a coupled system, and several complementary indicators are needed [109]. Apparent quantum efficiency (AQE, the ratio of reacting electrons to incident photons) reflects the utilization of light energy and can be measured at a defined wavelength and light intensity, allowing cross-system comparison of the intrinsic activity of the photocatalytic part; its value depends on the light spectrum, scattering, and reactor geometry, so the incident wavelength and the photon-flux measurement method must be stated [14]. PMS utilization efficiency,

defined as the amount of target degraded or mineralized per mole of PMS consumed, directly reflects oxidant economy and can be calculated from residual-PMS measurements, with related indicators including net oxidant utilization and reaction stoichiometric efficiency [110,111]; improving PMS utilization efficiency requires suppressing the self-scavenging side reaction between $SO_4^{\bullet-}$ and excess PMS, which is an important cause of the low mineralization efficiency of the radical route [112]. TOC removal reflects the degree of deep mineralization and is a necessary indicator of product toxicity and complete removal, and should be reported alongside the parent-compound degradation. Notably, not all coupled systems show positive synergy: when the PMS dosage is too high, or the illumination is mismatched, a negative synergy with SF below 1 can occur, in which case the above supplementary indicators more accurately reflect the practical value of the system [113].

7.3. Key Bottlenecks and Coping Strategies

As photocatalytic PMS-coupled systems advance toward practical applications, they encounter the challenge of addressing the coupled "triple bottleneck" of photochemistry and engineering. The first issue is the kinetic conflict between the recombination of photo-generated charge carriers and PMS activation. Although PMS serves as an electron acceptor that can enhance charge carrier separation, insufficient PMS concentration or adsorption rates result in charge carrier recombination becoming the dominant competitive process, which significantly reduces photocatalytic activity. Strategies to mitigate this bottleneck include accelerating interfacial electron transfer through atomic-level control methods, such as coordination engineering and defect modification [93], as well as developing carrier materials with a strong capacity for PMS adsorption.

Second, the long-term operational stability of photocatalysts presents a significant challenge. MOF-based and certain metal oxide catalysts exhibit susceptibility to photocorrosion and metal leaching when exposed to light and the oxidizing environment of PMS, resulting in a gradual decrease in catalytic activity. Surface protective layers, such as SiO_2 or carbon coatings, along with defect passivation techniques, effectively address this issue. For instance, a carbon-coated $CoFe_2O_4$ core-shell structure retains high catalytic activity even after multiple cycles.

Third, the engineering challenges associated with transitioning from laboratory-scale batch reactors to continuous-flow systems are significant. Currently, most photocatalytic PMS studies occur in idealized batch reactors, where pollutant concentrations typically range in the mg/L scale. However, the complex background components present in real wastewater matrices, including natural organic matter, anions, and suspended solids, exert a substantial quenching effect on reactive oxygen species (ROS). The development of continuous-flow photocatalytic membrane reactors, along with ultrasonic and microwave-assisted process intensification, has emerged as a key strategy for addressing these engineering bottlenecks [114].

7.4. Real Water Matrix Adaptability and Scale-Up Validation

Photocatalytic PMS-coupled systems are usually tested in pure water at mg/L pollutant levels, whereas anions, natural organic matter (NOM), and suspended solids in real water matrices interfere with reactive species and change degradation performance. Chloride is common in real water and is oxidized by $SO_4^{\bullet-}$ and •OH to generate reactive chlorine species (RCS) such as Cl• and $Cl_2^{\bullet-}$, whose redox potential and selectivity differ from those of $SO_4^{\bullet-}$; low Cl^- concentrations can promote degradation, whereas high concentrations quench radicals and may generate chlorinated by-products [115,116]. Bicarbonate and carbonate scavenge $SO_4^{\bullet-}$ and •OH to form carbonate radicals ($CO_3^{\bullet-}$), a weak oxidant, so that the removal of electron-rich pollutants is inhibited. The relative magnitude and direction of these effects depend on anion concentration, pH, and the dominant reactive species, so anion tolerance should be evaluated by concentration-gradient experiments in a real matrix rather than by pure-water kinetics alone.

NOM quenches $SO_4^{\bullet-}$ and •OH by competing for photons and radicals, and it also adsorbs on the catalyst surface to occupy active sites and further inhibits degradation; the resulting matrix effect is often the main reason that activity in real water falls below that in pure water [117]. Because NOM and inorganic anions act simultaneously, their combined effect cannot be extrapolated from single-component experiments, which highlights the need for systematic evaluation in real matrices.

Continuous-flow photocatalytic membrane reactors are an important route to engineering scale-up, but membrane fouling and catalyst leaching are the main obstacles. Fouling from NOM, colloids, and biomass covered the membrane surface, increases transmembrane pressure, and reduces permeate flux, while light screening by the cake layer reduces the photon flux reaching the photocatalyst. For immobilized catalysts, the loss of catalyst particles through detachment and metal leaching into the effluent raises the questions of whether the effluent meets discharge standards and whether the process is economically viable; a solution retaining low metal leaching and stable activity over a long-flow test has been reported, but such data are still scarce [118,119]. We recommend that future work report transmembrane-pressure rise, flux decline, catalyst-loss rate and the long-term change of leached-metal concentration together, so that membrane fouling and catalyst stability can be reasoned about jointly, and that a fouling-control and catalyst-regeneration protocol be adopted.

8. Conclusions and Outlook

This review systematically summarizes the research progress in antibiotic degradation in water through photocatalytic coupling with Persulfate (PMS) activation. It employs a three-dimensional analytical framework that includes "catalytic mechanism type, photocatalytic material system-reactive oxygen species generation pathway". The primary conclusions are as follows:

Classical pathways for activating Persulfate (PMS), including transition-metal catalysis, carbon-based material catalysis, physical energy field activation, and electrocatalysis, break O–O bonds in PMS through distinct physicochemical mechanisms. These processes primarily generate reactive oxygen species (ROS), such as $SO_4^{\bullet-}$, OH, and H_2O_2. The diversity and limitations of these mechanisms provide a crucial reference framework for assessing photocatalytic coupling pathways. Transition-metal catalysis demonstrates high efficiency but poses a risk of metal leaching. In contrast, carbon-based materials are environmentally friendly yet exhibit limited mineralization capacity. Physical activation operates under mild conditions but is energy-intensive, while electrocatalytic activation offers high controllability, although the costs associated with electrodes restrict its large-scale application.

The electron transfer mechanism for photocatalytic activation of PMS involves three progressive levels: thermodynamic band alignment, kinetic carrier separation, and radical/non-radical competition. The dual driving force of photo-generated electrons and holes offers unique advantages for PMS activation, distinguishing it from classical dark activation. Heterojunction engineering, including Type-II, Z-scheme, and S-scheme configurations, has significantly improved PMS activation efficiency through various carrier-separation strategies. Among these, the S-scheme heterojunction attains the optimal balance between strong redox capacity and separation efficiency. The three configurations differ systematically in PMS activation pathway selectivity, and the S-scheme advantage should be judged by actual radical/non-radical contributions rather than removal efficiency alone.

The introduction of monoatomic and diatomic catalysts advances the selective control of Persulfate (PMS) activation with atomic-level precision. The coordination environment of monoatomic sites determines the adsorption configuration of PMS and the pathway for O–O bond cleavage. Additionally, diatomic synergistic effects overcome the limitations imposed by the stoichiometric ratio of a single site, facilitating an electron transfer pathway that approaches 100%. This strategy exemplifies the forefront of catalyst design for PMS activation.

MOF/COF-based and metal-free photocatalysts provide tunable pore structures and environmentally friendly alternatives for PMS activation. However, their overall catalytic activity and long-term stability require significant improvement. Defect engineering and heteroatom doping serve as effective strategies for enhancing the performance of metal-free catalysts; nonetheless, their catalytic activity continues to lag considerably behind that of metal-based catalysts, which constitutes the primary bottleneck.

The primary advantage of photocatalytic PMS coupling is its capacity to achieve antibiotic degradation efficiencies that surpass those of conventional systems under near-neutral pH, room temperature, and low PMS dosage conditions. When SF is defined consistently and measured under identical conditions, the reported synergy factors of coupled systems span roughly 1.3 to 7, depending on the material, oxidant dose, and water matrix; cross-study comparison is meaningful only once definition and conditions are aligned. However, the main challenges involve three key aspects: low photonic quantum efficiency, inadequate long-term catalyst stability, and difficulties in scaling up for engineering applications. These factors represent significant barriers to translating laboratory advancements into practical applications.

In the coming decade, several areas are poised for significant advancements. High-throughput rational catalyst design, leveraging DFT calculations and machine learning, is anticipated to substantially reduce the time required for material discovery and performance validation through computational screening. Additionally, the integration and optimization of photocatalytic-coupled PMS processes will focus on real wastewater matrices, specifically addressing the quenching effects of coexisting ions and natural organic matter on reactive oxygen species (ROS) in actual wastewater, and will establish quantitative links between matrix indicators (anion type and concentration, NOM aromaticity, turbidity) and degradation performance through batch-to-continuous validation. Furthermore, engineering demonstrations of solar-driven, carbon-neutral photocatalytic water treatment technologies will use solar energy as the sole energy input, aiming for zero carbon emissions during the PMS activation process, while addressing membrane fouling control, catalyst regeneration, and replacing noble-metal co-catalysts with earth-abundant alternatives in real water treatment.

Statement of the Use of Generative AI and AI-Assisted Technologies in the Writing Process

During the preparation of this manuscript, the authors used ChatGPT to assist with language polishing and grammar correction. After using this tool, the authors reviewed, revised, and edited the full content of the manuscript. All authors take full responsibility for the content of this published article.

Acknowledgments

The authors thank the College of Chemistry and Chemical Engineering, Northwest Normal University, for providing administrative and technical support. This research received no specific grant from any funding agency beyond that declared in the Funding section.

Author Contributions

W.D.: investigation, writing—original draft; H.S.: writing-revised draft; X.W.: writing—original draft; Z.G.: visualization; Q.W.: conceptualization, funding acquisition. All authors reviewed the results and approved the final version of the manuscript.

Ethics Statement

Ethical review and approval were waived for this study, as it is a review article that does not involve humans or animals.

Informed Consent Statement

Not applicable.

Data Availability Statement

The datasets generated during and analyzed during the current study are available from the corresponding author on reasonable request.

Funding

This work was financially supported by the Key Research and Development Program of Gansu Province (24YFFA060) and the Lanzhou Science and Technology project (2025-2-106).

Declaration of Competing Interest

The authors declare that they have no known competing financial interests or personal relationships that could have appeared to influence the work reported in this paper.

References

1. Barkat H, Nasrullah AR, Hussain M, Sheikh NUA, Amjad N, Shi DD, et al. Next generation bismuth-based photocatalysts for emerging water contaminants: Design principles and future directions. *Coord. Chem. Rev.* **2026**, *562*, 217954. DOI:10.1016/j.ccr.2026.217954
2. Chen G, Yu Y, Liang L, Duan X, Li R, Lu X, et al. Remediation of antibiotic wastewater by coupled photocatalytic and persulfate oxidation system: A critical review. *J. Hazard. Mater.* **2021**, *408*, 124461. DOI:10.1016/j.jhazmat.2020.124461
3. Singh A, Majumder A, Saidulu D, Bhattacharya A, Bhatnagar A, Gupta AK. Oxidative treatment of micropollutants present in wastewater: A special emphasis on transformation products, their toxicity, detection, and field-scale investigations. *J. Environ. Manag.* **2024**, *354*, 120339. DOI:10.1016/j.jenvman.2024.120339
4. Sathish S, Madhu M, Muthu Prabhu S, Tseng WL. Emerging frameworks (MOFs/COFs) and selected carbon nanomaterials for the effective removal of per- and polyfluoroalkyl substances: Prospects and future directions. *Coord. Chem. Rev.* **2026**, *553*, 217560. DOI:10.1016/j.ccr.2025.217560
5. Huang Z, Hu LX, Yang JB, Liu YH, He LY, Liu YS, et al. Suspect and Nontarget Screening of Sulfonamides and Novel Transformation Products in Pharmaceutical Wastewater-Contaminated Areas: Distribution, Migration, and Environmental Risks. *Environ. Sci. Technol.* **2025**, *59*, 15978–15989. DOI:10.1021/acs.est.5c06191
6. Honarmandrad Z, Sun X, Wang Z, Naushad M, Boczkaj G. Activated persulfate and peroxymonosulfate based advanced oxidation processes (AOPs) for antibiotics degradation—A review. *Water Resour. Ind.* **2023**, *29*, 100194. DOI:10.1016/j.wri.2022.100194
7. Aftab M, Haq Khan ZU, Shah NS, Ullah F, Khasim S. Advanced oxidation processes for pesticide degradation: A comprehensive review on the role of nano zero-valent metals and persulfate activation. *RSC Adv.* **2025**, *15*, 40619–40654. DOI:10.1039/D5RA06043E
8. Ding Y, Wang X, Fu L, Peng X, Pan C, Mao Q, et al. Nonradicals induced degradation of organic pollutants by peroxydisulfate (PDS) and peroxymonosulfate (PMS): Recent advances and perspective. *Sci. Total Environ.* **2021**, *765*, 142794. DOI:10.1016/j.scitotenv.2020.142794
9. Kiejza D, Kotowska U, Polińska W, Karpińska J. Peracids—New oxidants in advanced oxidation processes: The use of peracetic acid, peroxymonosulfate, and persulfate salts in the removal of organic micropollutants of emerging concern—A review. *Sci. Total Environ.* **2021**, *790*, 148195. DOI:10.1016/j.scitotenv.2021.148195
10. Zhou X, Guo Z, Tang X, Wang W, Wu M, Song B, et al. Sulfate radical-based advanced oxidation processes for simultaneous removal of antibiotic-resistant bacteria and antibiotic resistance genes and the affecting factors. *Chem. Eng. J.* **2024**, *498*, 155149. DOI:10.1016/j.cej.2024.155149
11. Guo R, Bi Z, Xi B, Guo C, Zhang H, Lv N, et al. A new generation pathway of singlet oxygen in heterogeneous single-atom Mn catalyst/peroxymonosulfate system. *Chem. Eng. J.* **2024**, *481*, 148629. DOI:10.1016/j.cej.2024.148629
12. Song W, Li J, Fu C, Wang Z, Zhou Y, Zhang X, et al. Establishment of sulfate radical advanced oxidation process based on Fe^{2+}/O_2/dithionite for organic contaminants degradation. *Chem. Eng. J.* **2021**, *410*, 128204. DOI:10.1016/j.cej.2020.128204
13. Li N, Wang Y, Cheng X, Dai H, Yan B, Chen G, et al. Influences and mechanisms of phosphate ions onto persulfate activation and organic degradation in water treatment: A review. *Water Res.* **2022**, *222*, 118896. DOI:10.1016/j.watres.2022.118896

14. Wei Z, Yue X, Ji Y, Mu H, Wu L, Chen S, et al. Nanoarchitecture design for improved photocatalytic performance: A case study of titania mesocrystals modified with noble metals. *Appl. Catal. B Environ. Energy* **2026**, *383*, 126112. DOI:10.1016/j.apcatb.2025.126112
15. Ali S, Zuhra Z, Wang J. MOF-Derived Hollow CoFe@NC Nanocages for Highly Efficient Degradation of Textile Fibers. *Angew. Chem. Int. Ed.* **2026**, *65*, e6433467. DOI:10.1002/anie.6433467
16. Tripathy H, Balakrishnan A, Chinthala M, Kumar A. Peroxymonosulfate-activated photocatalytic reclamation of sulfamethoxazole using In_2S_3/CuSe infused carboxymethyl cellulose photocatalytic heterojunction hydrogels: Insights into operations and mechanisms. *Chem. Eng. J.* **2025**, *518*, 164360. DOI:10.1016/j.cej.2025.164360
17. Huang Z, Huang L, Fang S, Yang Y, Lai M, Zhong X, et al. Construction of Z-scheme C-$LaFeO_3$/Co-doped g-C_3N_4 heterojunction for synergistic photocatalysis-PMS activation in antibiotic degradation. *Chem. Eng. J.* **2026**, *537*, 176283. DOI:10.1016/j.cej.2026.176283
18. Ghanbari F, Moradi M. Application of peroxymonosulfate and its activation methods for degradation of environmental organic pollutants: Review. *Chem. Eng. J.* **2017**, *310*, 41–62. DOI:10.1016/j.cej.2016.10.064
19. Wang J, Wang S. Activation of persulfate (PS) and peroxymonosulfate (PMS) and application for the degradation of emerging contaminants. *Chem. Eng. J.* **2018**, *334*, 1502–1517. DOI:10.1016/j.cej.2017.11.059
20. Kohantorabi M, Moussavi G, Giannakis S. A review of the innovations in metal- and carbon-based catalysts explored for heterogeneous peroxymonosulfate (PMS) activation, with focus on radical *vs*. non-radical degradation pathways of organic contaminants. *Chem. Eng. J.* **2021**, *411*, 127957. DOI:10.1016/j.cej.2020.127957
21. Zheng X, Niu X, Zhang D, Lv M, Ye X, Ma J, et al. Metal-based catalysts for persulfate and peroxymonosulfate activation in heterogeneous ways: A review. *Chem. Eng. J.* **2022**, *429*, 132323. DOI:10.1016/j.cej.2021.132323
22. Zhao C, Shao B, Yan M, Liu Z, Liang Q, He Q, et al. Activation of peroxymonosulfate by biochar-based catalysts and applications in the degradation of organic contaminants: A review. *Chem. Eng. J.* **2021**, *416*, 128829. DOI:10.1016/j.cej.2021.128829
23. Luo J, Gao Y, Song T, Chen Y. Activation of peroxymonosulfate by biochar and biochar-based materials for degrading refractory organics in water: A review. *Water Sci. Technol.* **2021**, *83*, 2327–2344. DOI:10.2166/wst.2021.147
24. Li M, Li P, Zhou Q, Lee SLJ. A Mini Review on Persulfate Activation by Sustainable Biochar for the Removal of Antibiotics. *Materials* **2022**, *15*, 5832. DOI:10.3390/ma15175832
25. Dong C, Yi Q, He J, Xing M, Zhang J. Evolution of singlet oxygen in peroxymonosulfate activation: A review. *EES Catal.* **2023**, *1*, 103–116. DOI:10.1039/D2EY00107A
26. Gujar SK, Divyapriya G, Gogate PR, Nidheesh PV. Environmental applications of ultrasound activated persulfate/peroxymonosulfate oxidation process in combination with other activating agents. *Crit. Rev. Environ. Sci. Technol.* **2023**, *53*, 780–802. DOI:10.1080/10643389.2022.2085965
27. Li Y, Zhou Y, Zhou Y. Ultrasonic enhancement of persulfate oxidation system governs emerging pollutants decontamination. *Green Energy Environ.* **2024**, *9*, 1666–1678. DOI:10.1016/j.gee.2024.01.004
28. Wang L, Luo D, Hamdaoui O, Vasseghian Y, Momotko M, Boczkaj G, et al. Bibliometric analysis and literature review of ultrasound-assisted degradation of organic pollutants. *Sci. Total Environ.* **2023**, *876*, 162551. DOI:10.1016/j.scitotenv.2023.162551
29. Choi J, Lee D, Son Y. Ultrasonic activation of persulfate for removal of aqueous pollutants: Cavitational versus thermal mechanisms. *Curr. Opin. Chem. Eng.* **2025**, *48*, 101136. DOI:10.1016/j.coche.2025.101136
30. Anipsitakis GP, Dionysiou DD. Transition metal/UV-based advanced oxidation technologies for water decontamination. *Appl. Catal. B Environ.* **2004**, *54*, 155–163. DOI:10.1016/j.apcatb.2004.05.025
31. Chen R, Zhang H, Dong Y, Shi H. Dual metal ions/BNQDs boost PMS activation over copper tungstate photocatalyst for antibiotic removal: Intermediate, toxicity assessment and mechanism. *J. Mater. Sci. Technol.* **2024**, *170*, 11–24. DOI:10.1016/j.jmst.2023.07.005
32. Cui Y, Chen Z, Feng X, Ran X, Zhou S, Jiang F. Steering non-radical peroxymonosulfate activation via Au–S interfacial electronic engineering on defect-rich MIL-101(Fe)-NH_2: From radical suppression to singlet oxygen domination. *J. Clean. Prod.* **2026**, *568*, 148668. DOI:10.1016/j.jclepro.2026.148668
33. Zhou Q, Jiang B, Zhang L, Sun Y, Yang X, Zhang L. 1D/2D CoNi-LDH/$ZnIn_2S_4$ S-scheme heterojunction for effectively tetracycline degradation under photocatalytic-peroxymonosulfate activation system: DFT calculations and mechanism insights. *Chem. Eng. J.* **2023**, *478*, 147535. DOI:10.1016/j.cej.2023.147535
34. Bi Q, Zhang Y, Zhang C, Wang K, Zhao S, Xue J. Precise control of cobalt active site size to switch ROS pathways: Millimeter-scale carbon beads derived from dual MOFs for targeted degradation of drug pollutants. *Appl. Catal. B Environ. Energy* **2026**, *383*, 126046. DOI:10.1016/j.apcatb.2025.126046

35. Wang Z, Du M, Zhang Y, Qian Y, Chen Z, Qiu B, et al. Unlocking the potential of covalent organic frameworks: Fundamental investigation of molecular structures for in-situ H_2O_2 photosynthesis and antibiotic wastewater degradation. *Appl. Catal. B Environ. Energy* **2026**, *386*, 126435. DOI:10.1016/j.apcatb.2026.126435
36. Gao Y, Wang Q, Ji G, Li A. Degradation of antibiotic pollutants by persulfate activated with various carbon materials. *Chem. Eng. J.* **2022**, *429*, 132387. DOI:10.1016/j.cej.2021.132387
37. Zhang X, Yang X, Li Y, Li J, Zhang J, Zhang L, et al. Study on the mechanism of two-dimensional heterostructured interlayer-confined catalysts for efficient PMS activation in antibiotic degradation: Interface engineering and $^1O_2$ selective dominant pathway. *Chem. Eng. J.* **2025**, *521*, 166973. DOI:10.1016/j.cej.2025.166973
38. Li J, Wang D, Cheng K, Guan J, Wang L, Ma H, et al. Photothermal-assisted PMS activation via core-shell FeS_2/Bi_2MoO_6-OVs S-scheme heterojunction for efficient antibiotic degradation and algal inactivation. *Chem. Eng. J.* **2025**, *523*, 168768. DOI:10.1016/j.cej.2025.168768
39. Anipsitakis GP, Tufano TP, Dionysiou DD. Chemical and microbial decontamination of pool water using activated potassium peroxymonosulfate. *Water Res.* **2008**, *42*, 2899–2910. DOI:10.1016/j.watres.2008.03.002
40. Hong J, Dong J, Zhang X, Liu G, Li L, Wang B, et al. The synergistic effect of low concentration of peroxymonosulfate and visible light photocatalysis over FeOOH quantum dots/hollow g-C_3N_4 nanotubes S-scheme heterojunction for effectively antibiotics degradation. *J. Environ. Chem. Eng.* **2025**, *13*, 115777. DOI:10.1016/j.jece.2025.115777
41. Li Y, Chen L, Zhang J, Zhu C, Liu L. Synergistic photocatalytic degradation of TC-HCl by $Mn^{3+}/Co^{2+}/Bi_2O_3$ and PMS. *Inorg. Chem. Commun.* **2023**, *150*, 110468. DOI:10.1016/j.inoche.2023.110468
42. Peng Y, Tang H, Yao B, Gao X, Yang X, Zhou Y. Activation of peroxymonosulfate (PMS) by spinel ferrite and their composites in degradation of organic pollutants: A Review. *Chem. Eng. J.* **2021**, *414*, 128800. DOI:10.1016/j.cej.2021.128800
43. Oh D, Lee CS, Kang YG, Chang YS. Hydroxylamine-assisted peroxymonosulfate activation using cobalt ferrite for sulfamethoxazole degradation. *Chem. Eng. J.* **2020**, *386*, 123751. DOI:10.1016/j.cej.2019.123751
44. Li Y, Zhu W, Guo Q, Wang X, Zhang L, Gao X, et al. Highly efficient degradation of sulfamethoxazole (SMX) by activating peroxymonosulfate (PMS) with $CoFe_2O_4$ in a wide pH range. *Sep. Purif. Technol.* **2021**, *276*, 119403. DOI:10.1016/j.seppur.2021.119403
45. Ma T, Guo M, Cao Y, Zhong W, Ding C, Ye H, et al. Switch PMS activation pathway from free radical to non-radical by introducing hexagonal boron nitride in supported $CoFe_2O_4$: The role of lattice oxygen and PMS adsorption. *J. Environ. Chem. Eng.* **2024**, *12*, 114823. DOI:10.1016/j.jece.2024.114823
46. Si Y, Wang D, Han Y, Sun C, Xu L, Chen M. Modulating Fe sites by La in porous $MnFe_2O_4$ for enhanced removal of ROX: Synergy of efficient adsorption and PMS activation. *J. Hazard. Mater.* **2025**, *483*, 136600. DOI:10.1016/j.jhazmat.2024.136600
47. Chen W, Guo X, Xu Z, Wang J, Liu Z, Xie H, et al. Hydroxylamine enhanced peroxymonosulfate activation with $MnFe_2O_4$@NBC for naphthalene degradation: Performance and mechanism insights. *J. Water Process Eng.* **2025**, *73*, 107706. DOI:10.1016/j.jwpe.2025.107706
48. Zhang X, Yang X, Chen S, Dong S, Liu E, Li H, et al. Unravelling the synergy of Eu dopant and surface oxygen vacancies confined in bimetallic oxide for peroxymonosulfate activation. *Chem. Eng. J.* **2023**, *452*, 139192. DOI:10.1016/j.cej.2022.139192
49. Yang X, Wei G, Wu P, Liu P, Liang X, Chu W. Controlling oxygen vacancies of $CoMn_2O_4$ by loading on planar and tubular clay minerals and its application for boosted PMS activation. *J. Hazard. Mater.* **2022**, *436*, 129060. DOI:10.1016/j.jhazmat.2022.129060
50. Zhang L, Chen J, Zheng T, Xu Y, Liu T, Yin W, et al. Co–Mn spinel oxides trigger peracetic acid activation for ultrafast degradation of sulfonamide antibiotics: Unveiling critical role of Mn species in boosting Co activity. *Water Res.* **2023**, *229*, 119462. DOI:10.1016/j.watres.2022.119462
51. Wang L, Han C, Kong XY, Ye L, Huang Y. Piezoelectric Activation of Peroxymonosulfate by $CoMn_2O_4$ for Highly Efficient Tetracycline Degradation. *Langmuir* **2025**, *41*, 755–764. DOI:10.1021/acs.langmuir.4c04040
52. Hu X, Wang J, Wang J, Deng Y, Zhang H, Xu T, et al. β particles induced directional inward migration of oxygen vacancies: Surface oxygen vacancies and interface oxygen vacancies synergistically activate PMS. *Appl. Catal. B Environ.* **2022**, *318*, 121879. DOI:10.1016/j.apcatb.2022.121879
53. Zhang Q, Xu S, Fan Q, Zhang J, Zhou X, Sheng T, et al. Strain effect of Co-Mn spinel oxides boosts efficient peroxymonosulfate activation for water decontamination. *J. Environ. Chem. Eng.* **2026**, *14*, 122002. DOI:10.1016/j.jece.2026.122002

54. Wang J, Yao J, Yin L, Wang B, Liu X, Yuan L, et al. Facet engineering of metal-organic frameworks for efficient tetracycline degradation by photocatalytic activation of peroxymonosulfate. *Chem. Eng. J.* **2024**, *497*, 154836. DOI:10.1016/j.cej.2024.154836
55. Cheng X, Guo H, Zhang Y, Wu X, Liu Y. Non-photochemical production of singlet oxygen via activation of persulfate by carbon nanotubes. *Water Res.* **2017**, *113*, 80–88. DOI:10.1016/j.watres.2017.02.016
56. Hao L, Zhang J, Liu J, Min Y, Chen C. Applications of Carbon-Based Materials in Activated Peroxymonosulfate for the Degradation of Organic Pollutants: A Review. *Chem. Rec.* **2023**, *23*, e202300203. DOI:10.1002/tcr.202300203
57. Mady AH, Baynosa ML, Tuma D, Shim JJ. Heterogeneous activation of peroxymonosulfate by a novel magnetic 3D γ-MnO_2@$ZnFe_2O_4$/rGO nanohybrid as a robust catalyst for phenol degradation. *Appl. Catal. B Environ.* **2019**, *244*, 946–956. DOI:10.1016/j.apcatb.2018.11.086
58. Luo R, Li M, Wang C, Zhang M, Nasir Khan MA, Sun X, et al. Singlet oxygen-dominated non-radical oxidation process for efficient degradation of bisphenol A under high salinity condition. *Water Res.* **2019**, *148*, 416–424. DOI:10.1016/j.watres.2018.10.087
59. Zhang H, Gan X, Chen S, Yu H, Quan X. Non-doping 3D porous carbon with rich intrinsic defects for efficient nonradical activation of peroxymonosulfate toward the degradation of organic pollutants. *Sep. Purif. Technol.* **2022**, *292*, 121048. DOI:10.1016/j.seppur.2022.121048
60. Jiang M, Yang D, Wu J, Fan G. Nitrogen-doped hollow carbon spheres as efficient metal-free peroxymonosulfate activator for degradation of organic pollutant. *Diamond Relat. Mater.* **2024**, *141*, 110669. DOI:10.1016/j.diamond.2023.110669
61. Liu S, Pan Q, Li J, Wang M, Zhang J, Song Y, et al. Enhanced Mediated Electron Transfer Pathway of Peroxymonosulfate Activation Dominated with Graphitic-N for the Efficient Degradation of Various Organic Contaminants in Multiple Solutions. *ACS EST Water* **2022**, *2*, 817–829. DOI:10.1021/acsestwater.1c00495
62. Liu S, Lai C, Zhou X, Zhang C, Chen L, Yan H, et al. Peroxydisulfate activation by sulfur-doped ordered mesoporous carbon: Insight into the intrinsic relationship between defects and $^1O_2$ generation. *Water Res.* **2022**, *221*, 118797. DOI:10.1016/j.watres.2022.118797
63. Peng W, Liao J, Yan Y, Chen L, Ge C, Lin S. Enriched nitrogen-doped carbon derived from expired drug with dual active sites as effective peroxymonosulfate activator: Ultra-fast sulfamethoxazole degradation and mechanism insight. *Chem. Eng. J.* **2022**, *446*, 137407. DOI:10.1016/j.cej.2022.137407
64. Tian S, Xu Y, Ma Y, Jiang S, Ma J, Lin Y, et al. Exploring the electron transfer regime occurring in peroxides activation by graphite: Origin, mechanism and efficiency in complicated water matrices. *Chem. Eng. J.* **2024**, *485*, 150016. DOI:10.1016/j.cej.2024.150016
65. Wei Z, Villamena FA, Weavers LK. Kinetics and Mechanism of Ultrasonic Activation of Persulfate: An *In Situ* EPR Spin Trapping Study. *Environ. Sci. Technol.* **2017**, *51*, 3410–3417. DOI:10.1021/acs.est.6b05392
66. Zuo S, Li D, Xu H, Xia D. An integrated microwave-ultraviolet catalysis process of four peroxides for wastewater treatment: Free radical generation rate and mechanism. *Chem. Eng. J.* **2020**, *380*, 122434. DOI:10.1016/j.cej.2019.122434
67. Kuang C, Zeng G, Zhou Y, Wu Y, Li D, Wang Y, et al. Integrating anodic sulfate activation with cathodic H_2O_2 production/activation to generate the sulfate and hydroxyl radicals for the degradation of emerging organic contaminants. *Water Res.* **2023**, *229*, 119464. DOI:10.1016/j.watres.2022.119464
68. Li D, Zhang S, Li S, Tang J, Hua T, Li F. Mechanism of the application of single-atom catalyst-activated PMS/PDS to the degradation of organic pollutants in water environment: A review. *J. Clean. Prod.* **2023**, *397*, 136468. DOI:10.1016/j.jclepro.2023.136468
69. Hu J, Tian J, Yang Y, Li S, Lu J. Enhanced antibiotic degradation via photo-assisted peroxymonosulfate over graphitic carbon nitride nanosheets/$CuBi_2O_4$: Highly efficiency of oxygen activation and interfacial charge transfer. *J. Colloid Interface Sci.* **2024**, *661*, 68–82. DOI:10.1016/j.jcis.2024.01.135
70. Tong Y, Huang S, Zhao X, Yang Y, Feng L, Han Q, et al. Peroxymonosulfate activation by boron doped C_3N_5 metal-free materials with n → π* electronic transitions for tetracycline degradation under visible light: Insights into the generation of reactive species. *Chem. Eng. J.* **2024**, *480*, 147693. DOI:10.1016/j.cej.2023.147693
71. Wang A, Zhu BZ, Huang CH, Zhang WX, Wang M, Li X, et al. Generation mechanism of singlet oxygen from the interaction of peroxymonosulfate and chloride in aqueous systems. *Water Res.* **2023**, *235*, 119904. DOI:10.1016/j.watres.2023.119904
72. Zuo S, Xia D, Guan Z, Yang F, Zhang B, Xu H, et al. The polarized electric field on Fe_2O_3/g-C_3N_4 for efficient peroxymonosulfate activation: A synergy of $^1O_2$, electron transfer and pollutant oxidation. *Sep. Purif. Technol.* **2021**, *269*, 118717. DOI:10.1016/j.seppur.2021.118717

73. Zhu KA, Chen XJ, Yuan CW, Bai CW, Sun YJ, Zhang BB, et al. Orientated construction of visible-light-assisted peroxymonosulfate activation system for antibiotic removal: Significant enhancing effect of Cl^-. *J. Hazard. Mater.* **2023**, *445*, 130476. DOI:10.1016/j.jhazmat.2022.130476
74. Xu M, Lu M, Yang Y, Ai L, Fan H, Guo N, et al. Efficient degradation of pollutants by Bi_2WO_6/BiOCl heterojunction activated peroxymonosulfate: Performance and mechanism. *J. Environ. Chem. Eng.* **2024**, *12*, 112156. DOI:10.1016/j.jece.2024.112156
75. Zhang BB, Bai CW, Chen XJ, Sun YJ, Yang Q, Chen F. 2D/2D heterojunctions for rapid and self-cleaning removal of antibiotics via visible light-assisted peroxymonosulfate activation: Efficiency, synergistic effects, and applications. *J. Hazard. Mater.* **2024**, *468*, 133816. DOI:10.1016/j.jhazmat.2024.133816
76. Wang L, Lan X, Peng W, Wang Z. Uncertainty and misinterpretation over identification, quantification and transformation of reactive species generated in catalytic oxidation processes: A review. *J. Hazard. Mater.* **2021**, *408*, 124436. DOI:10.1016/j.jhazmat.2020.124436
77. Wang J, Wang S. Reactive species in advanced oxidation processes: Formation, identification and reaction mechanism. *Chem. Eng. J.* **2020**, *401*, 126158. DOI:10.1016/j.cej.2020.126158
78. Yang Y, Banerjee G, Brudvig GW, Kim JH, Pignatello JJ. Oxidation of Organic Compounds in Water by Unactivated Peroxymonosulfate. *Environ. Sci. Technol.* **2018**, *52*, 5911–5919. DOI:10.1021/acs.est.8b00735
79. Yun ET, Lee JH, Kim J, Park HD, Lee J. Identifying the Nonradical Mechanism in the Peroxymonosulfate Activation Process: Singlet Oxygenation Versus Mediated Electron Transfer. *Environ. Sci. Technol.* **2018**, *52*, 7032–7042. DOI:10.1021/acs.est.8b00959
80. Wang L, Li J, Liu X, Zhang J, Zeng P, Song Y. Overestimation of $^1O_2$ role in N-doped carbon materials/peroxymonosulfate system: The misleading of furfuryl alcohol quenching effect. *Chemosphere* **2023**, *324*, 138264. DOI:10.1016/j.chemosphere.2023.138264
81. Nosaka Y, Nosaka AY. Generation and Detection of Reactive Oxygen Species in Photocatalysis. *Chem. Rev.* **2017**, *117*, 11302–11336. DOI:10.1021/acs.chemrev.7b00161
82. Fu Y, Zhao Q, Wang Y, Su R, Li X, Liu R, et al. Enhancing peroxymonosulfate activation via $MnFe_2O_4$/MoS_2 S-scheme heterojunction for efficient photodegradation of ofloxacin: DFT calculations and mechanism insights. *Sep. Purif. Technol.* **2026**, *401*, 138561. DOI:10.1016/j.seppur.2026.138561
83. Wang Y, Xu D, Yang X, He JH. Novel 2D/2D S-scheme heterojunction photocatalyst for peroxymonosulfate activation enables ciprofloxacin ultrafast degradation: High-efficiency photogenerated carrier transport. *Chem. Eng. J.* **2024**, *488*, 150844. DOI:10.1016/j.cej.2024.150844
84. Yang Y, Hu P, Chen T, Yang S, Dong Z, Guo H, et al. Enhanced and synergistic photocatalytic peroxymonosulfate activation driven by S-scheme heterojunction for water purification: Redox cycle and oxygen vacancy effects. *Chem. Eng. J.* **2026**, *538*, 176697. DOI:10.1016/j.cej.2026.176697
85. Nie C, Wang X, Lu P, Zhu Y, Li X, Tang H. Advancements in S-scheme heterojunction materials for photocatalytic environmental remediation. *J. Mater. Sci. Technol.* **2024**, *169*, 182–198. DOI:10.1016/j.jmst.2023.06.011
86. Xu Q, Zhang L, Cheng B, Fan J, Yu J. S-Scheme Heterojunction Photocatalyst. *Chem* **2020**, *6*, 1543–1559. DOI:10.1016/j.chempr.2020.06.010
87. Kou L, Lei J, Jia J, Li Q, Zhang S, Tian Z, et al. A metal-free Z-scheme PPy/MCN heterojunction for antibiotic removal via synergism of photocatalysis and peroxymonosulfate activation. *Sep. Purif. Technol.* **2025**, *353*, 128573. DOI:10.1016/j.seppur.2024.128573
88. Gao Y, Liu YZ, Wang WL, Wu QY. Recent advances in the single-atom catalysts for persulfate activation and pollutant oxidation: A review. *J. Clean. Prod.* **2023**, *397*, 136576. DOI:10.1016/j.jclepro.2023.136576
89. Zhou D, Li Z, Hu X, Chen L, Zhu M. Single Atom Catalyst in Persulfate Oxidation Reaction: From Atom Species to Substance. *Small* **2024**, *20*, e2311691. DOI:10.1002/smll.202311691
90. Wang C, Wang X, Wang H, Zhang L, Wang Y, Dong CL, et al. Low-coordinated Co–N_3 sites induce peroxymonosulfate activation for norfloxacin degradation via high-valent cobalt-oxo species and electron transfer. *J. Hazard. Mater.* **2023**, *455*, 131622. DOI:10.1016/j.jhazmat.2023.131622
91. Li X, Wen X, Lang J, Wei Y, Miao J, Zhang X, et al. CoN_1O_2 Single-Atom Catalyst for Efficient Peroxymonosulfate Activation and Selective Cobalt(IV)=O Generation. *Angew. Chem. Int. Ed.* **2023**, *62*, e202303267. DOI:10.1002/anie.202303267
92. Deng Y, Ye YX, He Y, Xu J, Ke Z, Zhang X, et al. Highly effective activation of peroxymonosulfate via oxygen-coordinated single-atom iron for water decontamination. *Chem. Eng. J.* **2024**, *485*, 149782. DOI:10.1016/j.cej.2024.149782

93. Hu J, Zou Y, Li Y, Xiao Y, Li M, Lin L, et al. Efficacy and mechanism of peroxymonosulfate activation by single-atom transition metal catalysts for the oxidation of organic pollutants: Experimental validation and theoretical calculation. *J. Colloid Interface Sci.* **2023**, *645*, 1–11. DOI:10.1016/j.jcis.2023.04.093
94. Zeng Q, Wen Y, Duan X, Xu X, Tan J, Zhang Q, et al. Single-atom Ni–N_4 sites coordinate dual nonradical oxidation pathways via peroxymonosulfate activation: Computational insights and *in situ* spectroscopic analyses. *Appl. Catal. B Environ. Energy* **2024**, *346*, 123752. DOI:10.1016/j.apcatb.2024.123752
95. Zhou C, Liang Y, Xia W, Almatrafi E, Song B, Wang Z, et al. Single atom Mn anchored on N-doped porous carbon derived from spirulina for catalyzed peroxymonosulfate to degradation of emerging organic pollutants. *J. Hazard. Mater.* **2023**, *441*, 129871. DOI:10.1016/j.jhazmat.2022.129871
96. Zhao HQ, Song JS, Lu P, Mu Y. Single atom Co-anchored nitrogen-doped graphene for peroxymonosulfate activation with high selectivity of singlet oxygen generation. *Chem. Eng. J.* **2023**, *456*, 141045. DOI:10.1016/j.cej.2022.141045
97. Zhu C, Cun F, Fan Z, Nie Y, Du Q, Liu F, et al. Heterogeneous Fe–Co dual-atom catalyst outdistances the homogeneous counterpart for peroxymonosulfate-assisted water decontamination: New surface collision oxidation path and diatomic synergy. *Water Res.* **2023**, *241*, 120164. DOI:10.1016/j.watres.2023.120164
98. Hu J, Li Y, Zou Y, Lin L, Li B, Li XY. Transition metal single-atom embedded on N-doped carbon as a catalyst for peroxymonosulfate activation: A DFT study. *Chem. Eng. J.* **2022**, *437*, 135428. DOI:10.1016/j.cej.2022.135428
99. Yang M, Hou Z, Zhang X, Gao B, Li Y, Shang Y, et al. Unveiling the Origins of Selective Oxidation in Single-Atom Catalysis via Co–N_4–C Intensified Radical and Nonradical Pathways. *Environ. Sci. Technol.* **2022**, *56*, 11635–11645. DOI:10.1021/acs.est.2c01261
100. Liu X, Pei Y, Cao M, Yang H, Li Y. Highly dispersed copper single-atom catalysts activated peroxymonosulfate for oxytetracycline removal from water: Mechanism and degradation pathway. *Chem. Eng. J.* **2022**, *450*, 138194. DOI:10.1016/j.cej.2022.138194
101. Li Z, Ji X, Li Q, Zhen Y, Zhu S, Xu X, et al. Asymmetric Coordination Engineering of MXene-Based Metal Arrays for Oriented Generation of High-Valent Metal-Oxo Species from Peroxymonosulfate for Fast Water Decontamination. *Angew. Chem. Int. Ed.* **2026**, *65*, e22714. DOI:10.1002/anie.202522714
102. Chen J, Liu X, JiKe A, Liu Z, Zhang L, Jin Z, et al. Cobalt single-atom/cluster synergy for precision water decontamination: Unlocking a nearly 100% electron-transfer pathway in peroxymonosulfate activation. *J. Hazard. Mater.* **2026**, *503*, 141095. DOI:10.1016/j.jhazmat.2026.141095
103. Ijaz I, Bukhari A, Shaheen A, Nazir A, Gilani E, Zain H, et al. Activation of persulfate, peroxymonosulfate, and peroxydisulfate using metal-organic framework catalysts for degradation of antibiotics: Identification, quantification, interconversion, and transformation of reactive species. *J. Environ. Chem. Eng.* **2024**, *12*, 112838. DOI:10.1016/j.jece.2024.112838
104. Yin R, Chen Y, He S, Li W, Zeng L, Guo W, et al. *In situ* photoreduction of structural Fe(III) in a metal–organic framework for peroxydisulfate activation and efficient removal of antibiotics in real wastewater. *J. Hazard. Mater.* **2020**, *388*, 121996. DOI:10.1016/j.jhazmat.2019.121996
105. Fan Y, Zhang W, He K, Wang L, Wang Q, Liu J. Half-salen Fe(III) covalently post-modified MIL-125(Ti)-NH_2 MOF for effective photocatalytic peroxymonosulfate activation. *Appl. Surf. Sci.* **2022**, *591*, 153115. DOI:10.1016/j.apsusc.2022.153115
106. Liu X, Zhou J, Liu D, Liu S. Co isomorphic substitution for Cu-based metal organic framework based on electronic structure modulation boosts Fenton-like process. *Sep. Purif. Technol.* **2023**, *306*, 122526. DOI:10.1016/j.seppur.2022.122526
107. Xu Y, Xia P, Wang C, Cai J, Li H, Ye Z, et al. A mini-review on MOFs activated peroxide processes and the enhancement with the external energy. *Chem. Eng. J.* **2023**, *462*, 142021. DOI:10.1016/j.cej.2023.142021
108. Wu S, Shen L, Lin Y, Yin K, Yang C. Sulfite-based advanced oxidation and reduction processes for water treatment. *Chem. Eng. J.* **2021**, *414*, 128872. DOI:10.1016/j.cej.2021.128872
109. Cabrera-Reina A, Martínez-Piernas AB, Bertakis Y, Xekoukoulotakis NP, Agüera A, Sánchez Pérez JA. TiO_2 photocatalysis under natural solar radiation for the degradation of the carbapenem antibiotics imipenem and meropenem in aqueous solutions at pilot plant scale. *Water Res.* **2019**, *166*, 115037. DOI:10.1016/j.watres.2019.115037
110. Wang P, Zhang H, Wu Z, Zhao X, Sun Y, Duan N, et al. A data-based review on norfloxacin degradation by persulfate-based advanced oxidation processes: Systematic evaluation and mechanisms. *Chin. Chem. Lett.* **2023**, *34*, 108722. DOI:10.1016/j.cclet.2023.108722
111. Chen Y, Zeng B, Lai L, Luo L, Xie P, Shao Q, et al. Sulfite activation using FeO as a source of ferrous ions for fluoxetine degradation: A collaborated experimental and DFT study. *Chem. Eng. J.* **2022**, *441*, 135960. DOI:10.1016/j.cej.2022.135960

112. Wang S, Wang J. A novel strategy of successive non-radical and radical process for enhancing the utilization efficiency of persulfate. *Chemosphere* **2020**, *245*, 125555. DOI:10.1016/j.chemosphere.2019.125555
113. Dinesh GK, Chakma S. Mechanistic investigation in degradation mechanism of 5-Fluorouracil using graphitic carbon nitride. *Ultrason. Sonochem.* **2019**, *50*, 311–321. DOI:10.1016/j.ultsonch.2018.09.032
114. Sun Q, Wang X, Liu Y, Zhang Y, Xia S, Zhao J. Visible-light-driven g-C_3N_4 doped $CuFe_2O_4$ floating catalyst enhanced peroxymonosulfate activation for sulfamethazine removal via singlet oxygen and high-valent metal-oxo species. *Chem. Eng. J.* **2023**, *455*, 140198. DOI:10.1016/j.cej.2022.140198
115. Li W, Orozco R, Camargos N, Liu H. Mechanisms on the Impacts of Alkalinity, pH, and Chloride on Persulfate-Based Groundwater Remediation. *Environ. Sci. Technol.* **2017**, *51*, 3948–3959. DOI:10.1021/acs.est.6b04849
116. Liu Y, He X, Duan X, Fu Y, Fatta-Kassinos D, Dionysiou DD. Significant role of UV and carbonate radical on the degradation of oxytetracycline in UV-AOPs: Kinetics and mechanism. *Water Res.* **2016**, *95*, 195–204. DOI:10.1016/j.watres.2016.03.011
117. Li X, Wang J, Xia L, Cheng R, Chen J, Shang J. Peroxymonosulfate activation by nitrogen-doped herb residue biochar for the degradation of tetracycline. *J. Environ. Manag.* **2023**, *328*, 117028. DOI:10.1016/j.jenvman.2022.117028
118. Li N, Chen G, Zhao J, Yan B, Cheng Z, Meng L, et al. Self-cleaning PDA/ZIF-67@PP membrane for dye wastewater remediation with peroxymonosulfate and visible light activation. *J. Membr. Sci.* **2019**, *591*, 117341. DOI:10.1016/j.memsci.2019.117341
119. Zhang X, Xu S, Feng K, Li X, Yu P, Liu Q, et al. Fenton-like membrane reactor assembled by electron polarization and defect engineering modifying Co_3O_4 spinel for flow-through removal of organic contaminants. *Water Res.* **2024**, *254*, 121351. DOI:10.1016/j.watres.2024.121351